Statistical characterization of the anisotropic strain energy in soft materials with distributed fibers

Alessio Gizzi [a], Anna Pandolfi [b,*], Marcello Vasta [c]

[a] *Department of Engineering, University Campus Bio-Medico of Rome, Via A. del Portillo 21, Rome, 00128, Italy*
[b] *Dipartimento di Ingegneria Civile ed Ambientale, Politecnico di Milano, Piazza Leonardo da Vinci 32, Milano, Italy*
[c] *Dipartimento INGEO, Università di Chieti-Pescara, Viale Pindaro 42, Pescara, Italy*

We discuss analytical and numerical tools for the statistical characterization of the anisotropic strain energy density of soft hyperelastic materials embedded with fibers. We consider spa-tially distributed orientations of fibers following a tridimensional or a planar architecture. We restrict our analysis to material models dependent on the fourth pseudo-invariant I_4 of the Cauchy–Green tensor, and to exponential forms of the fiber strain energy function Ψ_{aniso}. Under different loading conditions, we derive the closed-form expression of the probability density function for I_4 and Ψ_{aniso}. In view of bypassing the cumbersome extension–contraction switch, commonly adopted for shutting down the contribution of contracted fibers in models based on generalized structure tensors, for significant loading conditions we identify analytically the support of the fibers in pure extension. For uniaxial loadings, the availability of the probability distribution function and the knowledge of the support of the fibers in extension yield to the analytical expression of average and variance of I_4 and Ψ_{aniso}, and to the direct definition of the average second Piola–Kirchhoff stress tensor. For generalized loadings, the dependence of I_4 on the spatial orientation of the fibers can be analyzed through angle plane diagrams. Angle plane diagrams facilitate the assessment of the influence of the pure exten-sion condition on the definition of the stable support of fibers for the statistics related to the anisotropic strain energy density.

Keywords:
Statistical fiber distribution
Fourth pseudo-invariant
Isochoric anisotropic hyperelasticity
Fiber reinforced materials

1. Introduction

In the last two decades soft tissue biomechanics and advanced constitutive modeling have been experiencing a growing research activity. The outcomes of this expanding impulse are glaring, since computational models of biological materials are now commonly used in tissue engineering design and development. Among others, well recognized examples of application can be found in cardiovascular functioning (Driessen et al., 2005), haemodynamics (Horgan and Saccomandi, 2003; Li and Robertson, 2009; Tsamis et al., 2013), damage and remodeling (Ferrara and Pandolfi, 2008; Ni Annaidh et al., 2012; Sánchez et al., 2014). As a consequence of the intrinsically *patient-specific* nature and of the microstructural complexity of biological tissues, their modeling is very challenging and still incomplete. The main difficulties are related to highly nonlinear behaviors and to inhomogeneities in the mechanical properties (Sacks, 2003).

Computational approaches for modeling the constitutive relations of biologic soft materials exhibiting reversibility rely on the definition of an appropriate strain energy density, eventually embedding, in a continuum sense, the underlying multiscale structure of the material. Within this perspective, microstructural constitutive models account for the

* Corresponding author. Tel.: +39 223994217.
E-mail address: anna.pandolfi@polimi.it (A. Pandolfi).

Published Journal Article available at: http://dx.doi.org/10.1016/j.mechmat.2015.09.008

List of symbols

$\mathbf{a}$:	fibers unit vector
$\mathbf{A}$:	fibers structure tensor
$\mathbf{H}$:	average fibers structure tensor
$\mathbb{H}$:	average fourth order structure tensor
Θ, Φ:	aleatoric Euler angles
θ, ϕ:	occurrence of the aleatoric Euler angles
I_4:	aleatoric fourth pseudo-invariant
I_4:	occurrence of the aleatoric fourth pseudo-invariant
λ:	imposed stretch
Ψ:	aleatoric anisotropic isochoric strain energy density
Ψ:	occurrence of the aleatoric anisotropic isochoric strain energy density
$\langle\mathbf{S}\rangle$:	average anisotropic stress tensor
$d\omega$:	spherical solid angle
$d\theta$:	planar angle increment
Ω:	unit sphere integration domain
$\mathcal{D}$:	generic integration domain
$\mathcal{D}_{\mathrm{F}}$:	extension–contraction integration domain
$\mathcal{D}_{\mathrm{E}}$:	pure-extension integration domain
$\rho(\mathbf{a})$:	generic probability distribution function
$\rho_\Theta(\theta)$:	probability distribution function of Θ
$\rho_{\mathrm{I}_4}(I_4)$:	probability distribution function of I_4
$\rho_\Psi(\Psi)$:	probability distribution function of Ψ
N_Θ:	normalization factor of $\rho_\Theta(\theta)$
N_{I_4}:	normalization factor of $\rho_{\mathrm{I}_4}(I_4)$
N_Ψ:	normalization factor of $\rho_\Psi(\Psi)$
I_4^*:	average fourth invariant
Ψ^*:	strain energy density evaluated at the average invariant $\Psi = \Psi(I_4^*)$
$\sigma^2_{I_4}$:	variance of I_4
σ^2_Ψ:	variance of Ψ
PDF:	probability distribution function

architecture and the spatial organization of the material structure by introducing explicitly their description in the strain energy density. A microstructural approach permits to better understand the physical significance of the material constants of the tissue, facilitating the achievement of a correct thus predictive macroscopic material model to be used in numerical applications.

To clarify the nature of the variability in the mechanical properties of fiber-reinforced soft tissues, Lanir (1983) introduced a stochastic approach within the definition of constitutive models. Lanir defined the strain energy density as the integral of the strain energy density of single fibers, spatially oriented according to a statistical distribution. Extensions and particular applications of this approach have been discussed in subsequent research (Holzapfel et al., 2000; Rodríquez et al., 2006; Alastrué et al., 2007; Federico and Gasser, 2010; Gizzi et al., 2014).

In spite of the large literature flourished from the seminal work of Lanir, we can acknowledge only a few attempts of characterizing analytically the statistical properties of the probability distribution functions (PDF) of complex materials showing an anisotropic microstructure. In particular, Zulliger et al. (2004) considered a log-logistic PDF for the progres-sive engagement of the fibers, while more recently Rodríquez et al. (2006) introduced a stochastic structural model de-scribing the waviness of a fiber bundle. The material model described in Rodríquez et al. (2006), derived from the worm-like chain model of Arruda and Boyce (1993), adopts a PDF of Beta type, calculated using Bayesian statistics but assuming a deterministic orientation of the fibers.

This study aims at characterizing analytically the statistics of mechanically significant quantities related to soft materials embedded with a stochastic distribution of reinforcing fibers. The presence of dispersed fibers confers to the medium a certain degree of anisotropy not easy to be described or quantified, whereas the availability of handy parameters would be highly desirable, especially in numerical applications. We consider hyperelastic materials, and restrict our consideration to isochoric behaviors. We assume that the anisotropic behavior of the material can be fully described by the fourth isochoric pseudo-invariant $\bar{I}_4$, which measures the square of the stretch in the direction of the fibers. Starting from a well established theoretical framework (Gasser et al., 2006; Pandolfi and Vasta, 2012; Vasta et al., 2014), we assume the tridimensional distribution of reinforcing fibers to be defined through of the composition of two PDFs associated to the Euler angles Θ and Φ, regarded as aleatoric variables. For uniaxial loading, we derive analytically the closed-form PDF of $\bar{I}_4$, as sole aleatoric variable defining the distribution, and, correspondingly, the PDF of the anisotropic strain energy density, Ψ_{aniso}. We identify the theoretically correct ranges of fiber in extension in terms of the meridian angle Θ for $\bar{I}_4$ and Ψ_{aniso}, by generalizing the approximate estimate recently proposed in Holzapfel and Ogden (2015), and we provide a better approximation of the average second Piola–Kirchhoff stress tensor. Furthermore, we discuss the implication of multiaxial loading on the range of fibers in extension, for tridimensional and planar distributions. We provide analytical forms of the PDFs and of their support for uniaxial and shear loadings, improving the computational efficiency of the stability condition for compressed fibers exclusion. For more general loadings, we illustrate how, from the observation of angle plane plots, it may be possible to define the range of fibers in extension, to be considered in the evaluation of the mechanically relevant statistics of the material.

The paper is organized as follows. In Section 2 we formulate the generalities of the material models for distributed fibers considered in this study and introduce the approximations for the strain energy density and stress tensor. In Section 3 we derive the closed-form PDF for the fourth pseudo-invariant and the anisotropic free energy density in the particular case of uniaxial loading in the direction of the fibers. More general loading conditions for tridimen-sional distributions of fibers are discussed in Section 4. In Section 5 we derive the PDFs for planar distributions of fibers. In Section 6 we present quantitative comparison between the mechanical response of our novel closed-form derivations and of alternative previous models. The results are discussed in Section 7. Limitations and future perspectives are drawn in Section 8.

2. Distributed fiber material models

In the following, according to the notation used in Holzapfel et al. (2000), we assume index notation for vectors and tensors and use the notation [**A**] to indicate the matrix representation of tensor **A** in a given basis. Moreover, we comply with the standard notation for random variables, thus denoting the random variable itself with non-italicized uppercase symbol (e.g., Θ, Φ, I_4, and W), and any particular realization of the random variable with italicized, when possible lowercase, symbol (e.g., θ, ϕ, I_4, and w) (Fisher et al., 1987).

We comply with the usual assumption of a strain energy density that decomposes additionally into three terms, fully decoupled by separation of arguments, i.e.,

$$\Psi = \Psi_{\mathrm{vol}} + \Psi_{\mathrm{iso}} + \Psi_{\mathrm{aniso}}.$$

The first term, $\Psi_{\mathrm{vol}} = \Psi_{\mathrm{vol}}(J)$, accounts for volume changes, and is dependent on the volumetric deformation expressed by the jacobian of the deformation gradient, $J = \det \mathbf{F}$. The second term, $\Psi_{\mathrm{iso}} = \Psi_{\mathrm{iso}}(\bar{I}_1, \bar{I}_2)$, accounts for the isochoric behavior of the isotropic constituents of the material, i.e., the matrix where the fibers are embedded, or for a portion of randomly distributed fibers. Usually the isotropic term is assumed to be dependent on the first and second invariants, $\bar{I}_1$ and $\bar{I}_2$, of the modified right Cauchy–Green deformation tensor $\bar{\mathbf{C}} = \bar{\mathbf{F}}^T\bar{\mathbf{F}}$, where $\bar{\mathbf{F}} = J^{-1/3}\mathbf{F}$. The third term, Ψ_{aniso}, addresses isochoric anisotropic behaviors and describes the effects of the fiber reinforcement. It is customary to assume that Ψ_{aniso} depends on the deformation through $\bar{\mathbf{C}}$ and on suitable structure tensors describing the fiber organization. Structure tensors are built considering the orientation of the fibers, characterized in the reference configuration by the unit vector **a**, in the form $\mathbf{A} = \mathbf{a} \otimes \mathbf{a}$. By disregarding the dependence on higher order invariants, the common assumption is that Ψ_{aniso} is dependent only on the fourth invariant $\bar{I}_4$ defined as

$$\bar{I}_4 = \mathbf{A} : \bar{\mathbf{C}}. \tag{1}$$

The physical meaning of $\bar{I}_4$ is the square of the stretch in the reference direction **a**. It is clear that in the case of contraction, a fiber will buckle and will not contribute to the stiffness of the material. Therefore, the expression of the material stress and stiffness should account for the fourth invariant (1) only for $\bar{I}_4 \geq 1$.

2.1. Anisotropic strain energy density

In the following we restrict our interest to the anisotropic part of the strain energy density, in the attempt of characterizing the statistical properties of the distribution of the reinforcement orientation. For a lighter notation, all the over bar will be removed from isochoric symbols, tensors and invariants, and Ψ will be used with the meaning of Ψ_{aniso}.

The choice of the functional form of Ψ is rather free; nevertheless, the exponential form adopted in Holzapfel et al. (2000) with reference to arterial walls shows mathematical properties that render it advantageous with respect to alter-native forms, and justify its wide popularity. Therefore we will refer to the form (Pandolfi and Vasta, 2012)

$$\Psi(I_4) = \frac{k_1}{2k_2}\exp\left[k_2(I_4 - 1)^2\right] - \frac{k_1}{2k_2}, \tag{2}$$

where the coefficient k_1 describes the fiber stiffness at low strains and k_2 controls the rigidity of the material at high strains. We observe that (2) can be solved explicitly with respect to I_4.

Let us consider a material point in a fibrous solid, the surrounding unit sphere Ω, and a generic orientation defined by the unit vector **a**, see Fig. 1(a). Fibers within Ω are spa-tially oriented according to a density $\rho(\mathbf{a})$, which quantifies the amount of fibers in the direction **a** and obeys the symme-try requirement $\rho(\mathbf{a}) \equiv \rho(-\mathbf{a})$. Given the orthogonal basis, $\mathbf{e}_1$, $\mathbf{e}_2$, and $\mathbf{e}_3$, and the spherical coordinates in the reference configuration, the unit vector **a** is expressed as

$$\mathbf{a}(\Theta, \Phi) = \sin\Theta\cos\Phi\,\mathbf{e}_1 + \sin\Theta\sin\Phi\,\mathbf{e}_2 + \cos\Theta\,\mathbf{e}_3,$$

where Θ and Φ are the Euler angles. The structure tensor **A** becomes

$$[\mathbf{A}] = \begin{bmatrix} \sin^2\Theta\cos^2\Phi & \sin^2\Theta\sin\Phi\cos\Phi & \sin\Theta\cos\Theta\cos\Phi \\ \sin^2\Theta\sin\Phi\cos\Phi & \sin^2\Theta\sin^2\Phi & \sin\Theta\cos\Theta\sin\Phi \\ \sin\Theta\cos\Theta\cos\Phi & \sin\Theta\cos\Theta\sin\Phi & \cos^2\Theta \end{bmatrix}. \tag{3}$$

We regard Θ and Φ as aleatoric variables varying in $[0, \pi]$, $[0, 2\pi]$, respectively. As usual in statistical descriptions, we denote with θ and ϕ, respectively, the occurrence of such variables. Given the infinitesimal solid angle $d\omega = \sin\theta\, d\theta d\phi$, the amount $\rho[\mathbf{a}(\theta, \phi)]d\omega$ represents the number of fibers whose orientation falls in the range $[(\theta, \theta + d\theta), (\phi, \phi + d\phi)]$. By definition of density, it follows that

$$\int_\Omega \rho\left[\mathbf{a}(\theta,\phi)\right] d\omega = \int_0^\pi \int_0^{2\pi} \rho\left[\mathbf{a}(\theta,\phi)\right] \sin\theta\, d\phi d\theta = 4\pi. \tag{4}$$

With reference to the considered distribution, the average operator $\langle\,\cdot\,\rangle$ is defined as

$$\langle\cdot\rangle \equiv \frac{1}{4\pi}\int_\omega \rho(\mathbf{a})(\,\cdot\,)\, d\omega, \tag{5}$$

and the average fourth pseudo-invariant is computed as

$$I_4^* \equiv \langle \mathrm{I}_4(\mathbf{a})\rangle = \frac{1}{4\pi}\int_\omega \rho(\mathbf{a})(\mathbf{A} : \mathbf{C})\, d\omega = \langle\mathbf{A}\rangle : \mathbf{C}, \tag{6}$$

where $\mathbf{H} = \langle\mathbf{A}\rangle$ is the average second order structure tensor introduced in Gasser et al. (2006). Accordingly, the average anisotropic strain energy density $\langle\Psi\rangle$ is computed as

$$\langle\Psi\rangle = \frac{1}{4\pi}\int_\omega \rho(\mathbf{a})\Psi(I_4)\, d\omega. \tag{7}$$

2.2. Transversely isotropic distributions of fibers

In view of applications in soft biological tissues, we assume the fiber distribution to be characterized by rotational symmetry about a mean referential direction, $\mathbf{a}_0$. In particular, we consider π-periodic distributions (Gasser et al., 2006) and, without loss of generality, we take the mean direction $\mathbf{a}_0$ to coincide with the unit vector $\mathbf{e}_3$, see Fig. 1(a).

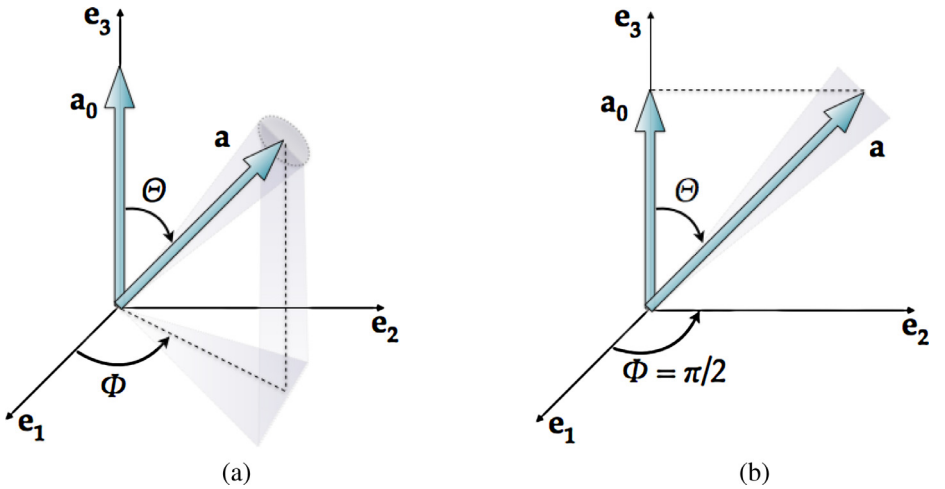

Fig. 1. Orientation of the generic unit vector **a** aligned with a portion of fibers in spherical coordinates for (a) a fully three-dimensional distribution and (b) a planar distribution of fibers in the plane $\mathbf{e}_2$, $\mathbf{e}_3$.

Rotational symmetry confers a transversely isotropic character to the overall response of the material. Within this framework, the joint PDF $\rho_{\Theta,\Phi}(\theta,\phi)$[1] that describes the density of fiber orientation $\rho[\mathbf{a}(\theta,\phi)]$ can be recast as

$$\rho_{\Theta,\Phi}(\theta,\phi) = \rho_{\Theta}(\theta)\,\frac{1}{2\pi}\,. \tag{8}$$

Accordingly, the normalization condition (4) reduces to

$$\frac{1}{2}\int_0^{\pi} \rho_{\Theta}(\theta)\,\sin\theta\,d\theta = 1.$$

The symmetric generalized structure tensor **H** becomes

$$\mathbf{H} = \langle \mathbf{A} \rangle\,, \quad [\mathbf{H}] = \begin{bmatrix} \kappa & 0 & 0 \\ 0 & \kappa & 0 \\ 0 & 0 & 1-2\kappa \end{bmatrix}, \tag{9}$$

where the coefficient κ is defined as

$$\kappa = \frac{1}{4}\int_0^{\pi} \rho_{\Theta}(\theta)\,\sin^3\theta\,d\theta. \tag{10}$$

2.3. Random transformation

A general expression of the PDF for the random variable[2] I_4 can be obtained from the PDF of the Euler angles through a random transformation procedure (Casella and Berger, 2008; Mardia and Jupp, 2000). The procedure requires the introduction of a new aleatoric variable W, with occurrence w, such that an inverse transformation is uniquely defined as

$$\begin{cases} \mathrm{I}_4 = \mathrm{I}_4(\Theta,\Phi) \\ \mathrm{W} = \Phi \end{cases} \quad \Leftrightarrow \quad \begin{cases} \Theta = \Theta(\mathrm{I}_4,\mathrm{W}) \\ \Phi = \mathrm{W} \end{cases} \tag{11}$$

[1] Given two random variables X and Y defined on a probability space, the joint probability distribution for X and Y (also called bivariate distribution) is a probability distribution that gives the probability that each X and Y falls in a particular range of values specified for X and Y, respectively.

[2] As already said, we denote with I_4 and W the random variables, and with I_4 and w the particular occurrence of the random variable.

and characterized by the jacobian

$$[\mathbf{J}_s] = \begin{bmatrix} \frac{\partial \mathrm{I}_4}{\partial\Theta} & \frac{\partial \mathrm{I}_4}{\partial\Phi} \\ \frac{\partial \mathrm{W}}{\partial\Theta} & \frac{\partial \mathrm{W}}{\partial\Phi} \end{bmatrix} = \begin{bmatrix} \frac{\partial \mathrm{I}_4}{\partial\Theta} & \frac{\partial \mathrm{I}_4}{\partial\Phi} \\ 0 & 1 \end{bmatrix}, \quad \det\mathbf{J}_s = \frac{\partial \mathrm{I}_4}{\partial\Theta}.$$

Referring to the new set of aleatoric variables I_4 and W, the general property of probability distributions becomes

$$\rho_{\mathrm{I}_4,\mathrm{W}}(I_4,w)\,dI_4\,dw = \rho_{\Theta,\Phi}(\theta,\phi)\,\sin\theta\,d\theta\,d\phi, \tag{12}$$

and the joint probability of the new random variables is related to the joint probability of the old random variables as

$$\begin{aligned} \rho_{\mathrm{I}_4,\mathrm{W}}(I_4,w) &= \left.\frac{\rho_{\Theta,\Phi}(\theta,\phi)\,\sin\theta}{\det\mathbf{J}_s}\right|_{\substack{\theta=\theta(I_4,w)\\ \phi=w}} \\ &= \rho_{\Theta,\Phi}(\theta,\phi)\,\sin\theta\left(\frac{\partial I_4}{\partial\theta}\right)^{-1}\Bigg|_{\substack{\theta=\theta(I_4,w)\\ \phi=w}} \end{aligned} \tag{13}$$

Thus the PDF of I_4 is obtained by integrating $\rho_{\mathrm{I}_4,W}(I_4,w)$ over the whole range of W, i.e.,

$$\rho_{\mathrm{I}_4}(I_4) = \int_0^{2\pi} \rho_{\Theta,\Phi}(\theta,\phi)\,\sin\theta\left(\frac{\partial I_4}{\partial\theta}\right)^{-1}\Bigg|_{\substack{\theta=\theta(I_4,w)\\ \phi=w}} dw. \tag{14}$$

If we consider the case of transversely isotropic materials with a uniform distribution of the aleatoric variable Φ, cf. Eq. (8), the PDF in (14) becomes

$$\rho_{\mathrm{I}_4}(I_4) = \frac{1}{2\pi}\int_0^{2\pi} \rho_{\Theta}(\theta)\,\sin\theta\left(\frac{\partial I_4}{\partial\theta}\right)^{-1}\Bigg|_{\theta=\theta(I_4,w)} dw, \tag{15}$$

where in general I_4 will depend on both Euler angles, i.e., $\mathrm{I}_4(\Theta,\Phi)$. Under particular loading conditions, the fourth invariant will depend only on Θ, leading to the direct transformation

$$\mathrm{I}_4 = \mathrm{I}_4(\Theta) \quad \Leftrightarrow \quad \Theta = \Theta(\mathrm{I}_4),$$

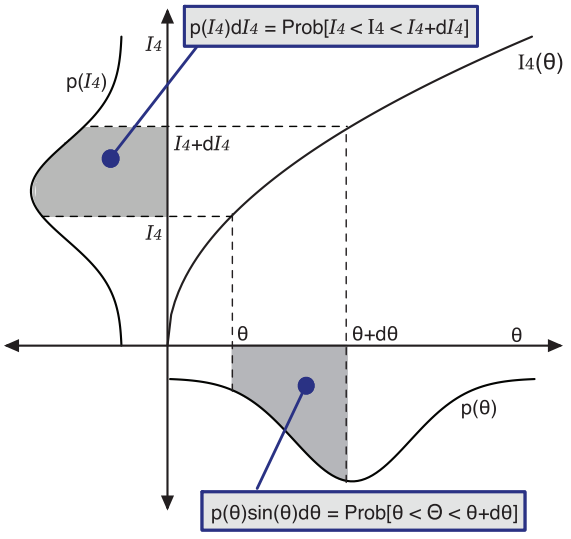

Fig. 2. Representative scheme for random variables transformation and the definition of the corresponding support.

for which Eq. (15) reduces to

$$\rho_{\mathrm{I}_4}(I_4) = \rho_\Theta(\theta)\,\sin\theta\left(\frac{\partial I_4}{\partial\theta}\right)^{-1}\Bigg|_{\theta=\theta(I_4)}. \tag{16}$$

A schematic interpretation of the random transformation procedure is shown in Fig. 2. Upon this transformation, consistency requires to use the PDF (15) in the definition of average I_4^*, variance $\sigma^2_{\mathrm{I}_4}$, and, in general, any further statistics of I_4, i.e.,

$$I_4^* \equiv \langle \mathrm{I}_4\rangle = \int_{\mathcal{D}} \rho_{\mathrm{I}_4}(I_4)\, I_4\, dI_4, \tag{17}$$

$$\sigma^2_{\mathrm{I}_4} \equiv \langle (\mathrm{I}_4 - I_4^*)^2\rangle = \int_{\mathcal{D}} \rho_{\mathrm{I}_4}(I_4)\,(I_4 - I_4^*)^2 dI_4, \tag{18}$$

where $\mathcal{D}$ denotes a suitable support of I_4.

2.4. Approximation of the anisotropic strain energy density and stress tensor

In hyperelasticity, the analytical form of the strain energy density leads to the analytical form of stress and elasticity tensors. Except very particular cases, for spatial distributions of the fiber orientation, $\langle\Psi\rangle$, as defined in Eq. (7), is not avail-able in analytical form, neither are the stress and the elas-ticity tensors. This can be a disadvantage, not only for com-putational reasons, but also because the features of the fiber distribution cannot be directly transferred to (and observed in) the stress and elasticity tensors. To subside this disadvan-tage, it is convenient to use approximated forms of the strain energy density.

Here, we comply with the approach proposed in Pandolfi and Vasta (2012), where the anisotropic strain energy density Ψ is assumed to be a function of the fourth invariant I_4 and is expanded in Taylor series about the average I_4^*, up to the second order terms. We refer to this expansion as *second order approximation*. The approximated from of the anisotropic strain energy density associated to the fibers in the direction Θ, e.g., the one reported in Eq. (2), is

$$\Psi(\mathrm{I}_4) \simeq \Psi^* + \Psi'^*(\mathrm{I}_4 - I_4^*) + \frac{1}{2}\Psi''^*(\mathrm{I}_4 - I_4^*)^2 \tag{19}$$

where

$$\Psi^* = \Psi(I_4^*) \quad \Psi'^* = \frac{\partial\Psi}{\partial I_4}\Bigg|_{I_4=I_4^*} \quad \Psi''^* = \frac{\partial^2\Psi}{\partial I_4\partial I_4}\Bigg|_{I_4=I_4^*}.$$

The average anisotropic strain energy density follows in analytical form as

$$\langle\Psi\rangle = \int_{\mathcal{D}} \rho_{\mathrm{I}_4}(I_4)\,\Psi(I_4)\,dI_4 = \Psi^* + \frac{1}{2}\,\Psi''^*\,\sigma^2_{I_4}. \tag{20}$$

Within the second order approximation, the definition of variance $\sigma^2_{I_4}$ requires the introduction of the additional coefficient

$$\hat\kappa = \frac{1}{16}\int_0^\pi \rho_\Theta(\theta)\,\sin^5\theta\,d\theta, \tag{21}$$

that accounts for higher order terms (cf. Pandolfi and Vasta, 2012). The average second Piola–Kirchhoff stress tensor follows as

$$\langle\mathbf{S}\rangle = 2\,\frac{\partial\langle\Psi\rangle}{\partial\mathbf{C}} = f\left(I_4^*,\sigma^2_{I_4}\right)\mathbf{H} + g\left(I_4^*,\sigma^2_{I_4}\right)\mathbb{H} : \mathbf{C}. \tag{22}$$

The fourth order tensor $\mathbb{H}$ in Eq. (22) depends on the coefficients κ and $\hat\kappa$. The definition of the tensor $\mathbb{H}$ can be found in Appendix A, together with the definition of the functions *f*, *g*, and of the non zero components of $\langle\mathbf{S}\rangle$.

In the following sections, we will derive the explicit expressions for the PDF of I_4 under particular conditions of loading, recurrent in applications of interest for transversely isotropic materials. As far as the numerical applications are concerned, we will assume $\rho_\Theta(\theta)$ to be a modified von Mises distribution, i.e., the projection of the normal distribution onto the unit sphere (Fisher et al., 1987). The modified von Mises distribution differs from the standard one regarding the normalization coefficient $N_\Theta(b)$ and reads

$$\rho_\Theta(\theta) = N_\Theta(b)\,\exp\left(b\cos 2\theta\right), \tag{23}$$

where

$$N_\Theta(b) = 4\sqrt{\frac{b}{2\pi}}\,\frac{\exp b}{\mathrm{erfi}(\sqrt{2b})},$$

$$\mathrm{erfi}(x) = -\frac{2\,\mathrm{i}}{\sqrt{\pi}}\int_0^{\mathrm{i}x}\exp\left(-t^2\right)dt$$

3. Uniaxial loading in the mean fiber direction

Uniaxial loading of the fibrous material is achieved by applying a stretch λ in the mean direction of the fiber orientation, see Fig. 3(a). For this loading, the fourth pseudo-invariant is a function only of the angle Θ. We wish to derive the reciprocal functional dependence between the two aleatoric variables Θ and I_4 and to find the expression of their PDFs. We begin without imposing the restriction on contracted fibers. The deformation gradient and the associated Cauchy–Green deformation tensor are

$$[\mathbf{F}] = \begin{bmatrix} \frac{1}{\sqrt{\lambda}} & 0 & 0 \\ 0 & \frac{1}{\sqrt{\lambda}} & 0, \\ 0 & 0 & \lambda \end{bmatrix} \quad [\mathbf{C}] = \begin{bmatrix} \frac{1}{\lambda} & 0 & 0 \\ 0 & \frac{1}{\lambda} & 0 \\ 0 & 0 & \lambda^2 \end{bmatrix}. \tag{24}$$

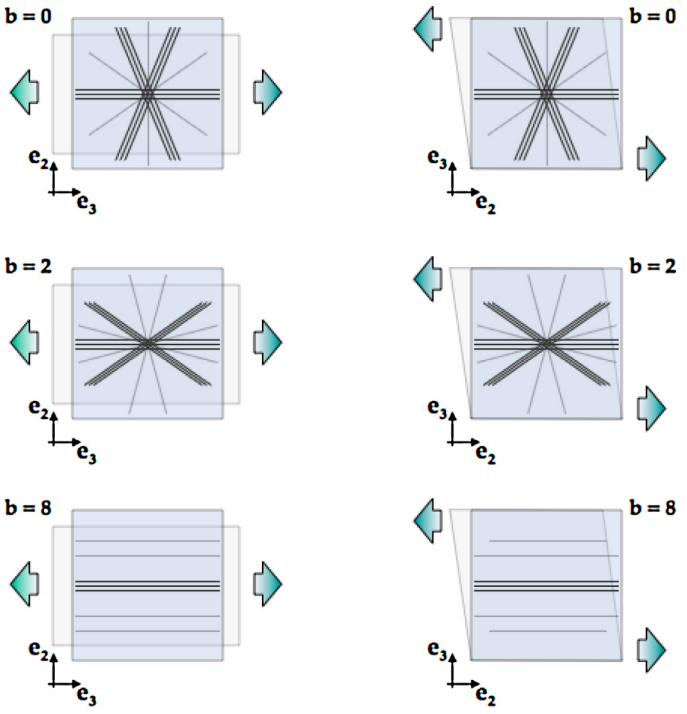

(a) Uniaxial (b) Simple shear

Fig. 3. Schematic of the basic loading cases, illustrating three values of the fiber concentration parameter b of the modified von Mises distribution. (a) Plane $\mathbf{e}_3$–$\mathbf{e}_2$, uniaxial loading in direction $\mathbf{e}_3$. (b) Plane $\mathbf{e}_2$–$\mathbf{e}_3$, simple shear cases.

The fourth pseudo-invariant written for the generic direction Θ becomes

$$\mathrm{I}_4 = \mathrm{I}_4(\Theta) = \frac{1}{\lambda} + \frac{\lambda^3 - 1}{\lambda} \cos^2 \Theta. \tag{25}$$

For a given λ, the function (25) can be solved with respect to Θ leading to

$$\Theta(\mathrm{I}_4) = \arccos \sqrt{\frac{\lambda\, \mathrm{I}_4 - 1}{\lambda^3 - 1}}. \tag{26}$$

As also discussed in Holzapfel and Ogden (2015), the enforcement of the local stability condition $\mathrm{I}_4 \geq 1$ restricts the variability of Θ to the intervals

$$\begin{aligned} &\arccos \frac{1}{\sqrt{1+\lambda+\lambda^2}} \leq \Theta \leq \pi \\ &\quad - \arccos \frac{1}{\sqrt{1+\lambda+\lambda^2}} \quad \text{if} \quad \lambda \leq 1\,, \\ &0 \leq \Theta \leq \arccos \frac{1}{\sqrt{1+\lambda+\lambda^2}} \cup \pi \\ &\quad - \arccos \frac{1}{\sqrt{1+\lambda+\lambda^2}} \leq \Theta \leq \pi \quad \text{if} \quad \lambda \geq 1\,, \end{aligned} \tag{27}$$

For uniaxial loading in the main direction of the fibers, Fig. 4 shows the dependence of I_4 versus Θ, see Eq. (25). The shadowed zones visualize the ranges of Θ for which fibers are in extension, i.e., $I_4 > 1$.Fig. 4(a,b) refer to an applied stretch $\lambda \leq 1$,$\lambda \geq 1$, respectively. Fig. 5(a) visualizes the contour levels of I_4 in the angle plane (Φ, Θ).

Restrictions (27) exclude the contribution of contracted fibers. Accounting for such restrictions, it is possible to compute the exact value of the parameters κ and $\hat{\kappa}$ defined in Eqs. (10)–(21) at an assigned stretch λ. The two parameters computed for the whole range of extended and contracted fibers have been reported first in Pandolfi and Vasta (2012). Fig. 6 shows the contraction free parameters κ and $\hat{\kappa}$ plot-ted versus the stretch λ and the concentration parameter b of the von Mises distribution. The contraction free parameters are affected sensibly by the imposed stretch λ, and the corresponding curves lay always below the ones that account for all the fibers. Original curves and contraction free curves coincide only for a strong alignment of the fibers (high values of b).

In the following section we prove that, by means of the derivation of the PDF of I_4, it is possible facilitate the satisfaction of the stability condition in the calculations.

3.1. PDF of the fourth pseudo-invariant

The PDF of the uniaxial I_4, Eq. (25), can be obtained by computing the derivative with respect to Θ of the inverse relation, Eq. (26), as

$$\frac{\partial \mathrm{I}_4}{\partial \Theta} = \frac{1-\lambda^3}{\lambda} \sin 2\Theta,$$

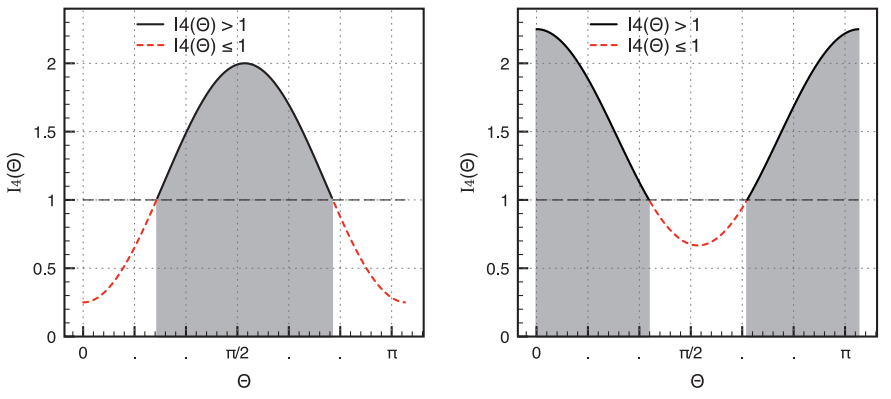

(a) $\lambda = 0.5$ (b) $\lambda = 1.5$

Fig. 4. Tridimensional distributions, uniaxial loading. Plot of $I_4(\Theta)$ in Eq. (25) for $\Theta \in [0{:}\ \pi]$ showing the admissible ranges of Θ accounting for extended fibers. (a) Uniaxial contraction stretch, $\lambda \leq 1$. (b) Uniaxial extension stretch, $\lambda \geq 1$.

and plugging it into Eq. (16). The closed-form expression of $\rho_{I_4}(I_4)$ for uniaxial loading follows as

$$\rho_{I_4}(I_4) = \frac{1}{N_{I_4}} \frac{\lambda}{\sqrt{\lambda^3 - 1}\sqrt{\lambda\, I_4 - 1}} \exp\left[b\left(2\frac{\lambda I_4 - 1}{\lambda^3 - 1} - 1 \right) \right], \tag{28}$$

where $N_{I_4}(\lambda, b)$ is a normalization factor. Eq. (28) shows that $\rho_{I_4}(I_4)$ is parametrized upon the applied stretch λ and the concentration parameter b.

The double dependence is demonstrated in Fig. 7 by three plots of $\rho_{I_4}(I_4)$, for different values of b and λ. The plots show that $\rho_{I_4}(I_4)$ tends to flatten over a large portion of the support when stretches are rather high. Fig. 7 visualizes the lower and upper limits of integration of the function $\rho_{I_4}(I_4)$, located at λ^{-1} and λ^2, respectively. Shadowed zones highlight the integration range of $I_4 \geq 1$. Note that λ^{-1} is also a singular point of the distribution: a vertical asymptote is present for any value of the parameter b. For $b \gg 1$ the asymptote is not visible due to negligible occurrences of the random variable. Contrari-wise, λ^2, is the absolute maximum value of the stretch under uniaxial loading conditions. Between the two limit points,
the PDF of I_4 is continuous and smooth. We take the two limit points to define the full support $\mathcal{D}_F \in]\lambda^{-1}, \lambda^2[$ of the $\rho_{I_4}(I_4)$. It follows that the normalization factor of $\rho_{I_4}(I_4)$ is defined as

$$N_{I_4} = \int_{\mathcal{D}_F} \frac{\lambda}{\sqrt{\lambda^3 - 1}\sqrt{\lambda\, I_4 - 1}} \exp b\left(2\frac{\lambda\, I_4 - 1}{\lambda^3 - 1} - 1 \right) dI_4. \tag{29}$$

Remark 3.1A. The above discussion holds for uniaxial loadings in the mean direction of the fibers, and the resulting PDF Eq. (28) does not discriminate between extended or contracted fibers.

Remark 3.1B. The two limit points coincide with the eigenvalues of **C**, see Eq. (24), one of which has multiplicity 2. In the case of uniaxial extension in the mean direction of the fibers, the two identical eigenvalues correspond to contractions, and viceversa.

3.2. PDF of the anisotropic strain energy density

We use the previous results to derive the analytical expression of the PDF of the anisotropic strain energy density Ψ, $\rho_\Psi(\Psi)$, for the uniaxial loading case. The awareness of the behavior of the strain energy density is of relevance in assessing the reliability of the outcomes of numerical simulations. Recalling the general property of probability distributions, we can write

$$\rho_{I_4}(I_4)\, dI_4 = \rho_\Psi(\Psi)\, d\Psi. \tag{30}$$

We refer to the particular exponential form of the anisotropic strain energy density given in (2), and solve it with respect to I_4 obtaining

$$I_4 = I_4(\Psi) = 1 + \sqrt{\frac{1}{k_2} \ln\left(1 + \frac{2k_2}{k_1}\Psi \right)}. \tag{31}$$

We derive $\rho_\Psi(\Psi)$ in closed-form from Eq. (30) using the general property of probability distributions as

$$\begin{aligned} \rho_\Psi(\Psi) &= \rho_{I_4}(I_4) \left(\frac{d\Psi}{dI_4} \right)^{-1} \\ &= \frac{1}{N_\Psi} \frac{\rho_{I_4}(I_4)}{k_1(I_4 - 1)\exp\left[k_2(I_4 - 1)^2 \right]} \Big|_{I_4 = I_4(\Psi)}, \end{aligned} \tag{32}$$

where I_4 has to be intended as a function of Ψ in the form (31), and $N_\Psi(\lambda, b)$ is a normalization factor. As expected, $\rho_{I_4}(I_4)$ and $\rho_\Psi(\Psi)$ share similar features. In particular, also $\rho_\Psi(\Psi)$ depends on the von Mises concentration parameter b and on the applied stretch λ. Representative examples of $\rho_\Psi(\Psi)$ for different values of b and λ are visualized in Fig. 8. The plots show that $\rho_\Psi(\Psi)$ does exist and is positive definite only for $\Psi > 0$. This observation is important for the definition of the requisite statistics of $\rho_\Psi(\Psi)$, which are meaningful only when referred to the positive range of Ψ.

Next, we wish to control the influence of $\rho_{I_4}(I_4)$ on $\rho_\Psi(\Psi)$ to exclude detrimental effects on the convexity of the anisotropic strain energy density, due to the presence of contracted fibers. To this aim, we refer to the extension and contraction conditions discussed in the definition of the PDF of

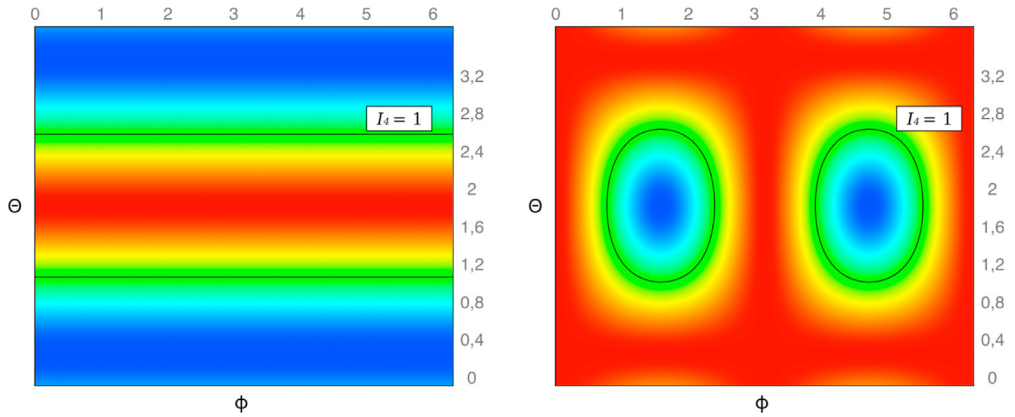

(a) Uniaxial, $\lambda = 1.5$ (b) Equibiaxial, $\lambda = 1.5$

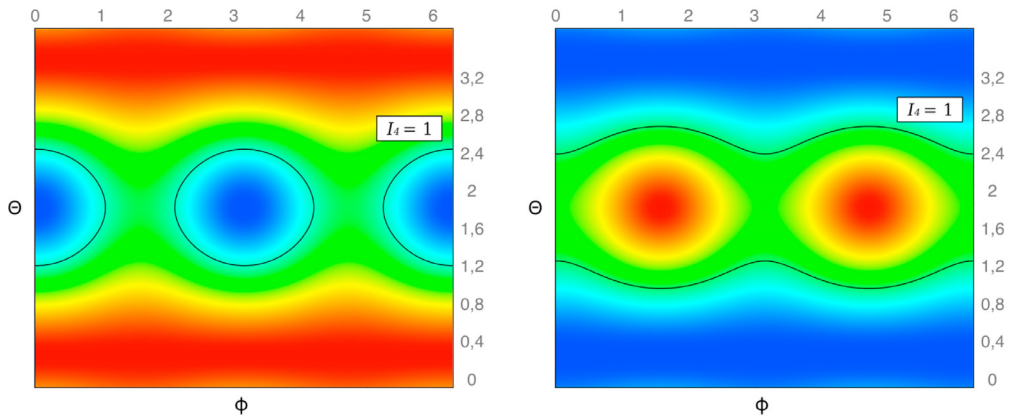

(c) Biaxial, $\lambda_1 = 1.5$, $\lambda_2 = 1.1$ (d) Biaxial, $\lambda_1 = 0.7$, $\lambda_2 = 1.3$

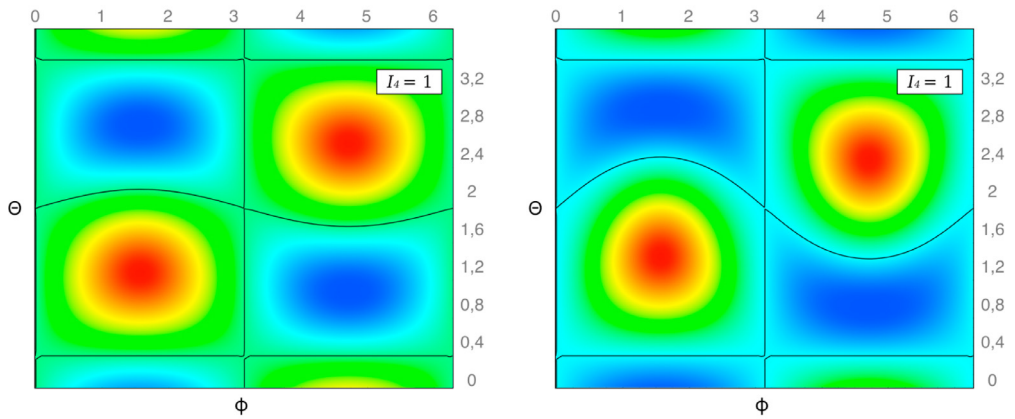

(e) Shear, $\gamma = 0.4$ (f) Shear, $\gamma = 1.2$

Fig. 5. Angle plane plots of $I_4(\Theta, \Phi)$ in the plane $[\Theta, \Phi] \in [0{:}\ \pi, 0{:}\ 2\pi]$. (a) Tridimensional distributions, uniaxial loading, Eq. (25) with $\lambda = 1.5$; (b) Tridimensional distributions, equibiaxial loading, Eq. (36) with $\lambda_1 = \lambda_2 = 1.5$; (c, d) Tridimensional distributions, biaxial loading Eq. (36) with $\lambda_1 = 1.5$, $\lambda_2 = 1.1$ and $\lambda_1 = 0.7$, $\lambda_2 = 1.3$, respectively; (e, f) Tridimensional distributions, shear loading Eq. (40) with $\gamma = 0.4$ and $\gamma = 1.2$, respectively. Color codes: red and blue for $I_4 \geq 1$ and $I_4 < 1$, respectively. Black solid lines indicate the contour level $I_4 = 1$. (For interpretation of the references to color in this figure legend, the reader is referred to the web version of this article.)

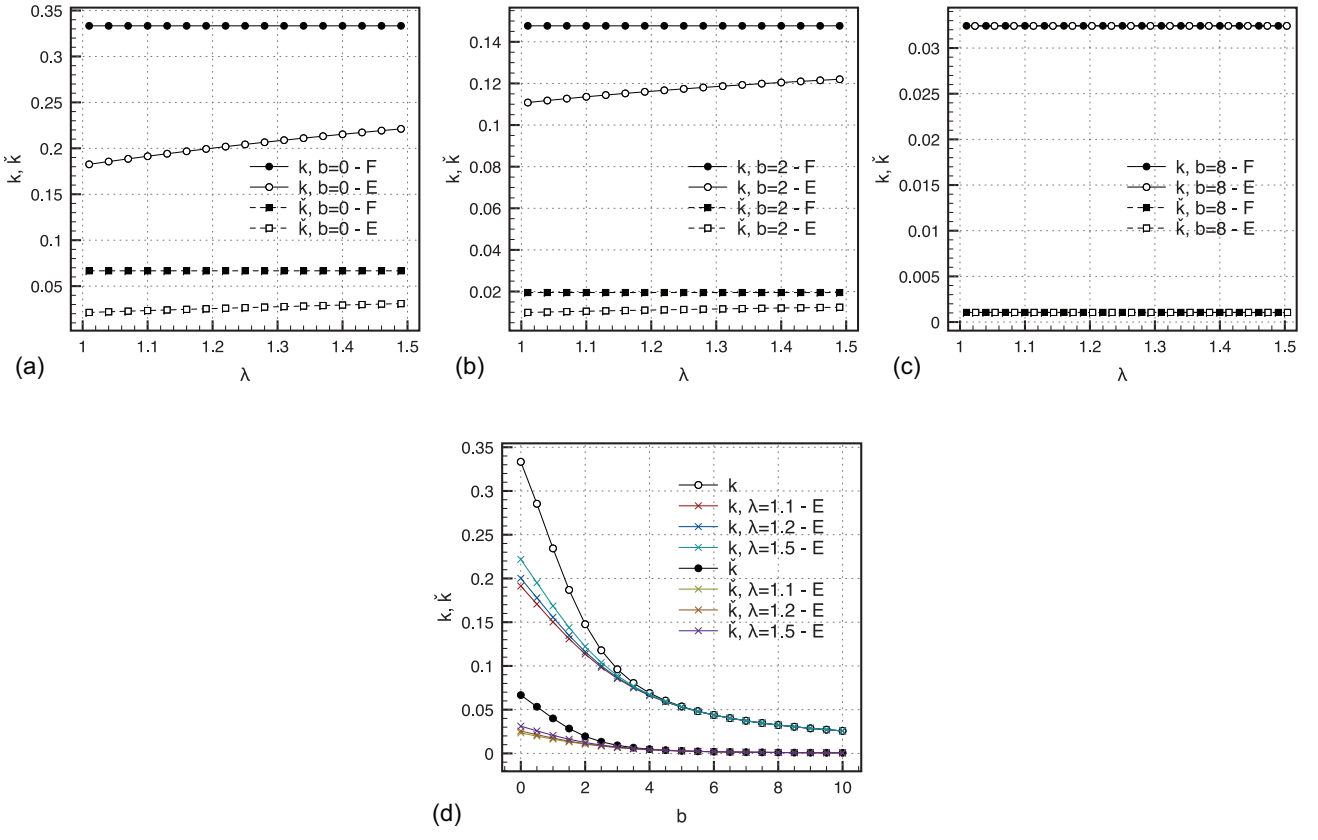

Fig. 6. Tridimensional distributions, uniaxial loading. Comparison between the variables κ and $\check{\kappa}$, Eqs. (10) and (21), respectively, computed for the full support $\Theta \in [0, \pi]$ (F) and the ones computed for Θ in the range accounting only for the extended fibers (E), see Eq. (27). (a–c) Variation versus λ for fixed values of the concentration parameter $b = 0, 2, 8$, respectively. (d) Variation versus b with respect to the stretch $\lambda = 1.1, 1.2, 1.5$, respectively.

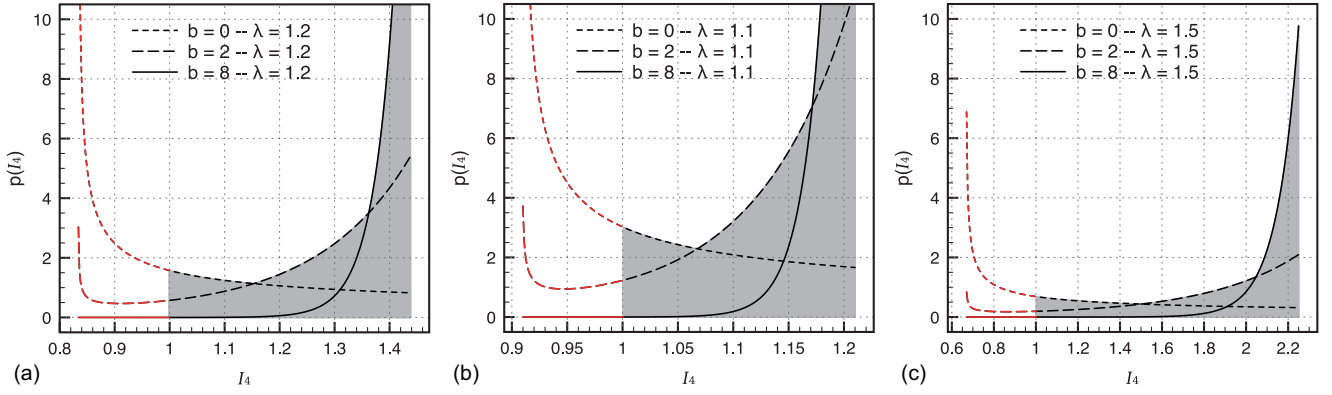

Fig. 7. Tridimensional distributions, uniaxial loading. Examples of $\rho_{I_4}(I_4)$ versus I_4, see Eq. (28), for three values of $b = 0, 2, 8$ and $\lambda = 1.1, 1.2, 1.5$. I_4 is defined within the range $]\lambda^{-1}, \lambda^2[$. The resulting PDFs flatten for high values of the stretch and concentrate towards the upper bound for increasing values of b. The integration range of $I_4 \geq 1$ is highlighted as shadow zones.

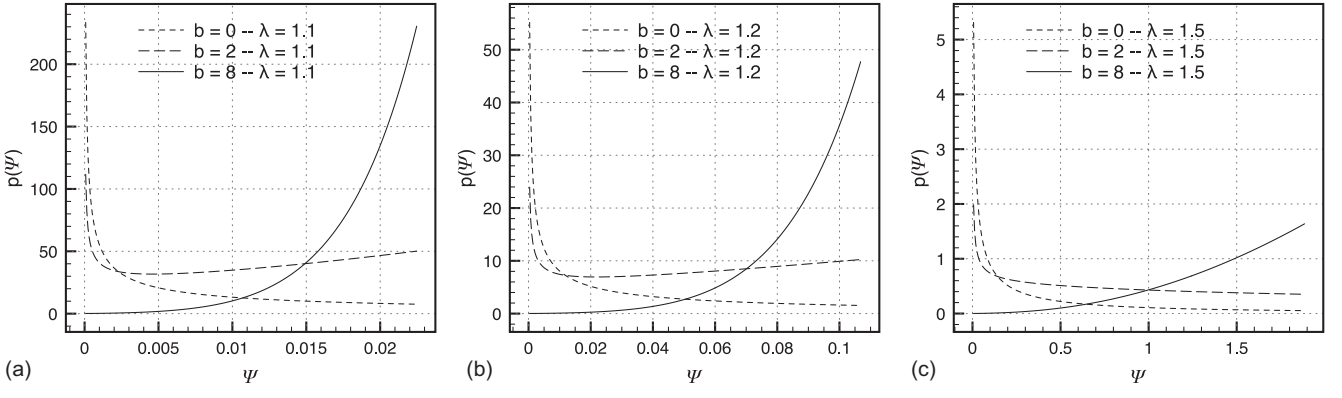

Fig. 8. Tridimensional distributions, uniaxial loading. Examples of $\rho_\Psi(\Psi)$ versus Ψ, see Eq. (32), for three values of $b = 0, 2, 8$ and $\lambda = 1.1, 1.2, 1.5$. Ψ is defined within the range $]0, \Psi(\lambda^2)[$. The resulting PDFs flatten for high values of the stretch and concentrate towards the upper bound for increasing values of b. In this case shadowed zones are not provided since the integration range starts from $\Psi = 0$.

I_4. The function $\rho_\Psi(\Psi)$ in Eq. (32) must consider only the physically admissible range of Ψ which accounts for fibers in extension, i.e., $\mathcal{D}_E \in]\Psi(1) \equiv 0,\ \Psi(\lambda^2)[$. Clearly, $\mathcal{D}_E$ varies with the assumed angular fiber distribution and the applied stretch, but only in the upper limit of the support. Accordingly, the normalization condition becomes

$$N_\Psi = \int_{\mathcal{D}_E} \frac{\rho_{I_4}(I_4(\Psi))}{k_1(I_4(\Psi)-1)\exp\left[k_2(I_4(\Psi)-1)^2\right]}\, d\Psi. \quad (33)$$

The knowledge of the extension support $\mathcal{D}_E$ permits the exact evaluation of all the statistics related to Ψ. In particular, the average and the variance of Ψ follow, with no approximations, as

$$\langle\Psi\rangle = \int_{\mathcal{D}_E} \rho_\Psi(\Psi)\,\Psi\, d\Psi, \quad (34)$$

$$\sigma_\Psi^2 = \langle\Psi - \Psi^*\rangle^2 = \int_{\mathcal{D}_E} \rho_\Psi(\Psi)(\Psi-\Psi^*)^2 d\Psi. \quad (35)$$

Remark 3.2A. The exponential form of the strain energy density allows to identify the unique inverse relation with the fourth pseudo-invariant. Moreover, the monotonicity of the exponential law allows to define $\rho_\Psi(\Psi)$ naturally within the physical support corresponding to the range of the extended fibres, where $I_4 \geq 1$.

Remark 3.2B. The knowledge of $\rho_\Psi(\Psi)$ in closed-form allows for the exact evaluation of all its statistics, Eqs. (34) and(35) in particular. We note that $\Psi^* \equiv \Psi(I^*_4) \neq \langle\Psi\rangle$.

4. General loadings for tridimensional fiber distributions

Under general loading conditions, the characterization of the PDF of tridimensional distributions of fibers becomes more difficult. Still restricting our considerations to the wide class of transversely isotropic materials, we derive the analytical form of the PDF of I_4 for general loadings making use of the general transformation rule for random variables recalled in Section 2.3. Additionally, we describe the PDF relationships in terms of angle plane, and clarify the analytical derivation by means of plots comparison and numerical calculations.

4.1. Biaxial loading

As in the uniaxial case, we take the direction $\mathbf{e}_3$ to be the mean orientation of the fibers, and take it to coincide with one of the principal directions of loading. A general biaxial loading characterized by two stretches λ_1 (in the mean fiber direction) and λ_2 (in the transversal plane) leads to the following deformation tensors

$$[\mathbf{F}] = \begin{bmatrix} \frac{1}{\lambda_1\lambda_2} & 0 & 0 \\ 0 & \lambda_2 & 0 \\ 0 & 0 & \lambda_1 \end{bmatrix}, \quad [\mathbf{C}] = \begin{bmatrix} \frac{1}{\lambda_1^2\lambda_2^2} & 0 & 0 \\ 0 & \lambda_2^2 & 0 \\ 0 & 0 & \lambda_1^2 \end{bmatrix}.$$

In this case, the fourth pseudo-invariant (1) depends on both the Euler angles Θ and Φ,

$$I_4(\Theta,\Phi) = \lambda_1^2 + F(\lambda_1,\lambda_2,\Phi)\sin^2\Theta, \quad (36)$$

where

$$F(\lambda_1,\lambda_2,\Phi) = \frac{1}{\lambda_1^2\lambda_2^2}\left[(1-\lambda_1^2\lambda_2^4)\cos^2\Phi + \lambda_1^2\lambda_2^2\left(\lambda_2^2-\lambda_1^2\right)\right].$$

The criterion $I_4 \geq 1$, which discriminates between extended and contracted fibres, does not lead to a straightforward identification of the support $\mathcal{D}_E$ of purely extended fibers. The definition of $\mathcal{D}_E$ requires, in this case, the composition of the joint probabilities of Θ and Φ.

We try to visualize the complex relationship (36) through the angle plane plots in Fig. 5(b–d). The contour levels of $I_4 = I_4(\Theta,\Phi)$ are reported for different values of the stretches. As in the uniaxial case, also in this case, the eigenvalues of $\mathbf{C}$ are the stationary points of I_4, i.e., λ_1^2, λ_2^2, and $1/\lambda_1^2\lambda_2^2$; according to the applied stretch values they identify the absolute maximum, the local maximum, and the absolute minimum of I_4. The stability limit ($I_4 = 1$) is visualized in Fig. 5 with a solid black contour level. The shape of the stability contour level changes markedly from a loading configuration to another, testifying the difficulty in achieving an unified analytical description for the stability support $\mathcal{D}_E$. It follows that the a priori identification of the angular ranges satisfying the stability condition $I_4 \geq 1$ becomes a complex problem dependent on the stretch ratio λ_2^2/λ_1^2.

In order to bypass such a difficulty, following the procedure described in Section 2.3, we introduce an auxiliary aleatoric variable W which coincides with the aleatoric variable Φ. The inverse relation becomes

$$\Theta(I_4, W) = \arcsin\sqrt{\frac{I_4-\lambda_1^2}{F(\lambda_1,\lambda_2,W)}}, \quad (37)$$

and the derivative of I_4 with respect to Θ is

$$\frac{\partial I_4}{\partial\Theta} = F(\lambda_1,\lambda_2,W)\sin 2\Theta. \quad (38)$$

The integral form of the PDF of I_4 under biaxial loading is obtained by substituting (37) and (38) in Eq. (15), as

$$\rho_{I_4}(I_4) = \frac{1}{2\pi}\frac{1}{N_\Theta}\int_0^{2\pi} \frac{\exp(b\cos 2\theta)}{2\cos\theta\, F(\lambda_1,\lambda_2,w)}\bigg|_{\theta=\theta(I_4,w)} dw, \quad (39)$$

where we implicitly assume the exclusion of the values of w not satisfying the existence conditions of Eq. (37). This result allows us to directly implement the stability condition $I_4 \geq 1$ without the necessity of complex integral paths as described for the angular PDFs.

The PDF in Eq. (39) is parametrized upon the concentration parameter b, the stretches λ_1, λ_2, and the fourth invariant I_4. Representative examples of $\rho_{I_4}(I_4)$ for three different values of b are shown in Fig. 9. As expected, in contrast with the previous case, the resulting PDF acquires more complex morphologies according to the different sets of parameters. In particular, for very dispersed distributions of the fibers ($b \simeq 0$) and for extension–contraction combination of stretches, the resulting PDF distributions are non-monotone and show an intermediate peak. For high values of b, corresponding to strongly aligned fiber distributions, the $\rho_{I_4}(I_4)$ shows the same side peak observed in the uniaxial loading

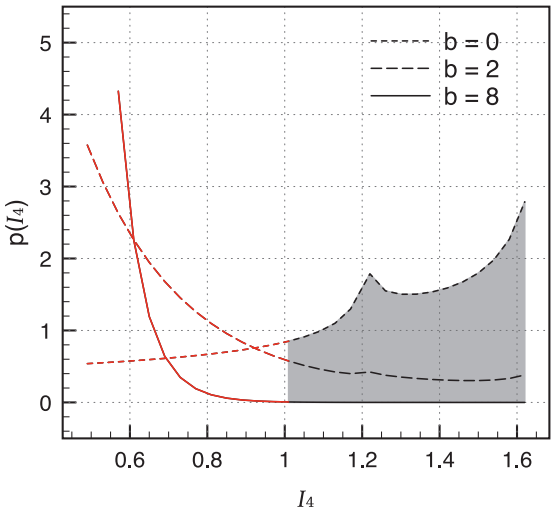

Fig. 9. Tridimensional distributions, biaxial loading. Examples of $\rho_{I_4}(I_4)$, Eq. (39) for three values of the concentration parameter $b = 0, 2, 8$. The stretches are set $\lambda_2 = 1.3$, $\lambda_1 = 0.7$ and correspond to the angle plane plot in Fig. 5(d). A multimodal shape is observed for low values of b. The resulting PDFs flatten and concentrate towards the lower bound for increasing values of b. The integration range of $I_4 \geq 1$ is highlighted as shadow zones.

case. Nonetheless, the integration range of $I_4 \geq 1$ is similar to the previous cases and highlighted by the shadowed zones.

Remark 4.1A. Fig. 9 shows $\rho_{I_4}(I_4)$ for all the possible occurrences of I_4, included the ones that do not satisfy the stability condition $I_4 \geq 1$. The stability condition in terms of the Euler angles is influenced by the specific values of the applied stretches in a manner that cannot be rendered explicitly. Also for the biaxial PDF, Eq. (39), in general, the stability condition $I_4 \geq 1$ can be enforced by limiting the support of $\rho_{I_4}(I_4)$.

Remark 4.1B. In the case of shear loading characterized by a parameter γ, the fourth invariant is expressed as

$$I_4(\Theta, \Phi) = 1 + \gamma \sin 2\Theta \sin \Phi + \gamma^2 \cos^2 \Theta. \tag{40}$$

The functional relation (40) becomes intricate and characterized by closed regions where $I_4 \geq 1$, cf. Fig. 5(e,f). As it can be grasped from the contour levels, in the simple shear load-ing case the application of the general procedure for random variable transformation becomes rather complicated. The full analysis of the PDF of I_4 requires the use of disjoint PDFs for Θ and Φ and the recourse to advanced and dedicated computational tools, which go beyond the aims of the present work.

5. Planar fiber distributions

Next, we restrict our considerations to planar distributions of fibers, by specializing the distribution density $\rho(\mathbf{a})$ according to the approach described in Wang et al. (2012); Vasta et al. (2014). We account for a π-periodic planar distribution lying on the plane normal to the direction $\mathbf{e}_1$, where $\Phi = \pi/2$, and, for the obvious symmetry $\rho(\mathbf{a}) = \rho(-\mathbf{a})$, we limit $\Theta \in [-\pi/2, \pi/2]$. It follows that $\rho(\mathbf{a}) = \rho_\Theta(\theta)$ is independent of the angle Φ. With no loss of generality, we assume the mean direction of the fiber orientation to coincide with the Cartesian basis vector $\mathbf{e}_3$, see Fig. 1(b). In contrast with the three-dimensional case, in a planar setting the quantity $\rho_\Theta(\theta)d\theta$ represents the amount of fibers lying in the direction Θ. The normalization condition (4) becomes

$$\frac{1}{\pi}\int_{-\pi/2}^{\pi/2} \rho_\Theta(\theta)d\theta = 1,$$

and the average operator is defined as

$$\langle\cdot\rangle = \frac{1}{\pi}\int_{-\pi/2}^{\pi/2} \rho_\Theta(\theta)(\,\cdot\,)d\theta.$$

Furthermore, the unit vector $\mathbf{a}$ shows a dependence only on the angle Θ

$$\mathbf{a}(\Theta) = \sin\Theta\,\mathbf{e}_2 + \cos\Theta\,\mathbf{e}_3,$$

as well as the structure tensor $\mathbf{A}$

$$[\mathbf{A}] = \begin{bmatrix} 0 & 0 & 0 \\ 0 & \sin^2\Theta & \sin\Theta\cos\Theta \\ 0 & \sin\Theta\cos\Theta & \cos^2\Theta \end{bmatrix}.$$

The average structure tensor has the explicit form

$$[\mathbf{H}] = \begin{bmatrix} 0 & 0 & 0 \\ 0 & \kappa & 0 \\ 0 & 0 & 1-\kappa \end{bmatrix}, \tag{41}$$

where

$$\kappa = \frac{1}{\pi}\int_{-\pi/2}^{\pi/2} \rho_\Theta(\theta)\,\sin^2\theta\,d\theta, \tag{42}$$

and the additional coefficient $\hat{\kappa}$ accounting for higher order terms becomes

$$\hat{\kappa} = \frac{1}{\pi}\int_{\pi/2}^{\pi/2} \rho_\Theta(\theta)\,\sin^4\theta\,d\theta \tag{43}$$

cf. (Vasta et al., 2014; Wang et al., 2012). The planar distri-bution allows to derive the explicit expressions for the PDF under uniaxial and simple shear deformation. We remind that, within a planar setting and under the incompressibility constraint, the uniaxial loading corresponds to a pure shear loading condition.

5.1. Uniaxial loading for planar distributions of fibers

We start by considering a uniaxial test in the plane $\mathbf{e}_2$–$\mathbf{e}_3$ of the fiber distribution, see Fig. 3(a). The deformation tensors assume the form

$$[\mathbf{F}] = \begin{bmatrix} 1 & 0 & 0 \\ 0 & 1/\lambda & 0 \\ 0 & 0 & \lambda \end{bmatrix}, \quad [\mathbf{C}] = \begin{bmatrix} 1 & 0 & 0 \\ 0 & 1/\lambda^2 & 0 \\ 0 & 0 & \lambda^2 \end{bmatrix},$$

leading to the following expression of I_4, i.e.,

$$I_4(\Theta) = \frac{1}{\lambda^2} + \left(\lambda^2 - \frac{1}{\lambda^2}\right)\cos^2\Theta. \tag{44}$$

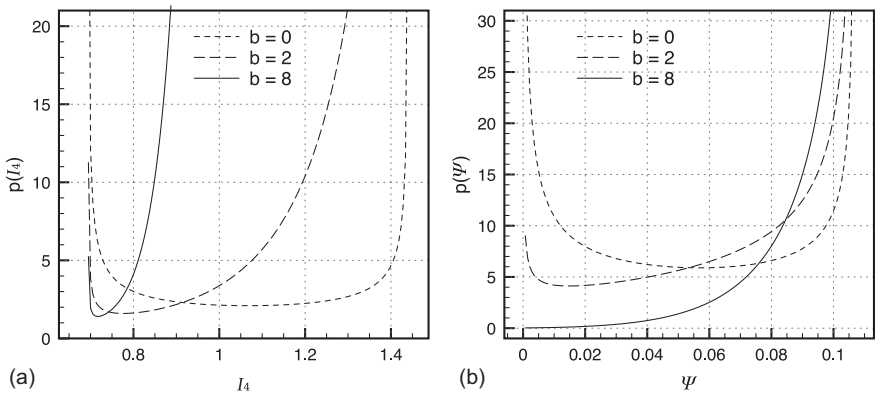

Fig. 10. Planar distributions, uniaxial loading. The stretch $\lambda = 1.2$ is applied for different values of the Mises concentration parameter $b = 0, 2, 8$. (a) Plot of $\rho_{I_4}(I_4)$ versus I_4, restricted to the range $]\lambda^{-2}, \lambda^2[$, see Eq. (46). The resulting PDFs show increased values of I_4 for increasing values of b due to the enforcement of the incompressibility constraint. (b) Plot of $\rho_\Psi(\Psi)$ versus Ψ, restricted to the range $]0, \Psi(\lambda^2)[$, see Eq. (47). The resulting PDFs of the energy show similar trends to the one reported in Fig. 8 for three-dimensional distributions.

For a given λ, Eq. (44) can be solved with respect to Θ as

$$\Theta(I_4) = \arccos\sqrt{\frac{\lambda^2 I_4 - 1}{\lambda^4 - 1}}\,.$$

The enforcement of the condition $I_4 \geq 1$ restricts the variability of Θ to the ranges

$$\begin{aligned} &-\arccos\frac{1}{\sqrt{1+\lambda^2}} < \Theta < \arccos\frac{1}{\sqrt{1+\lambda^2}} \quad \text{for} \quad \lambda > 1, \\ &-\frac{\pi}{2} < \Theta < -\arccos\frac{1}{\sqrt{1+\lambda^2}} \cup \\ &\quad \arccos\frac{1}{\sqrt{1+\lambda^2}} < \Theta < \frac{\pi}{2} \quad \text{for} \quad \lambda < 1\,. \end{aligned} \tag{45}$$

The relation $I_4 = I_4(\Theta)$ for uniaxial loading for planar fiber distributions is visualized in Fig. 11, where the shadowed re-gions represent the ranges of Θ leading to fiber extension. The kinematics of the uniaxial loading for planar distributions of fibers is very close to the one for tridimensional distributions shown in Fig. 4. In the planar setting, the increase in the values of I_4 derives from the enforcement of the incompressibility constraint. Consequently, the derivation of the PDFs follows the same steps illustrated for tridimensional distributions. The derivative of (44) with respect to Θ is, in particular,

$$\frac{dI_4}{d\Theta} = \left(\frac{1}{\lambda^2} - \lambda^2\right)\sin 2\Theta.$$

The expression of the PDF of I_4 under uniaxial loading in a planar setting becomes

$$\rho_{I_4} = \frac{1}{N_{I_4}}\frac{\lambda^2}{2\sqrt{\lambda^4-1}\sqrt{\lambda^2 I_4 - 1}}\exp\left[b\left(2\frac{\lambda^2 I_4 - 1}{\lambda^4 - 1} - 1\right)\right], \tag{46}$$

and the PDF of Ψ becomes

$$\rho_\Psi = \frac{1}{N_\Psi}\left.\frac{\rho_{I_4}(I_4)}{k_1(I_4-1)\,\exp\left[k_2(I_4-1)^2\right]}\right|_{I_4 = I_4(\Psi)}, \tag{47}$$

where we assume $I_4 = I_4(\Psi)$ as in Eq. (31). $N_{I_4}(\lambda, b)$ and $N_\Psi(\lambda, b)$ are the normalization factors, corresponding to Eqs. (29) and (33), respectively, in the case of tridimensional distributions. Eq. (46) shows that $\rho_{I_4}(I_4)$ is parametrized upon the applied stretch λ and the concentration param-eter b of the von Mises distribution. As in the tridimen-sional distribution case, the two limit points coincide with the eigenvalues of the Cauchy–Green deformation tensor, i.e., λ^{-2} and λ^2. Eqs. (47) and (32) have very similar functional form, indeed, the only difference given by the expression of the fourth pseudo-invariant PDF. In particular, $\rho_\Psi(\Psi)$ is uniquely defined for $\Psi > 0$; the support, accounting only for the fibers in extension, is limited to $\Psi(\lambda^2)$ in order to respect the upper bound condition of $\rho_{I_4}(I_4)$. Illustrative examples of $\rho_{I_4}(I_4)$ and $\rho_\Psi(\Psi)$ for planar distributions under uniaxial loading for different values of the concentration parameter b are shown in Fig. 10(a,b), respectively. The derivation of the approximated average stress follows the steps described in the previous section.

5.2. Simple shear loading in planar distributions of fibers

We conclude by analyzing the simple shear loading in the plane of the fibers, see Fig. 3(b), characterized by the following deformation tensors

$$[\mathbf{F}] = \begin{bmatrix} 1 & 0 & 0 \\ 0 & 1 & \gamma \\ 0 & 0 & 1 \end{bmatrix}, \quad [\mathbf{C}] = \begin{bmatrix} 1 & 0 & 0 \\ 0 & 1 & \gamma \\ 0 & \gamma & 1+\gamma^2 \end{bmatrix}.$$

The associated pseudo-invariant I_4 is

$$I_4(\Theta) = 1 + \gamma\sin 2\Theta + \gamma^2\cos^2\Theta. \tag{48}$$

Relation (48) is visualized in Fig. 12. The ranges of Θ identifying extended fibers are uniquely defined by the intervals

$$\begin{aligned} &-\frac{\pi}{2} < \Theta < \arctan\frac{\gamma}{2} \quad \text{for } \gamma < 0, \\ &-\arctan\frac{\gamma}{2} < \Theta < \frac{\pi}{2} \quad \text{for } \gamma > 0, \end{aligned} \tag{49}$$

The derivative of the invariant (48) with respect to Θ is

$$\frac{dI_4}{d\Theta} = 2\gamma\cos 2\Theta - \gamma^2\sin 2\Theta.$$

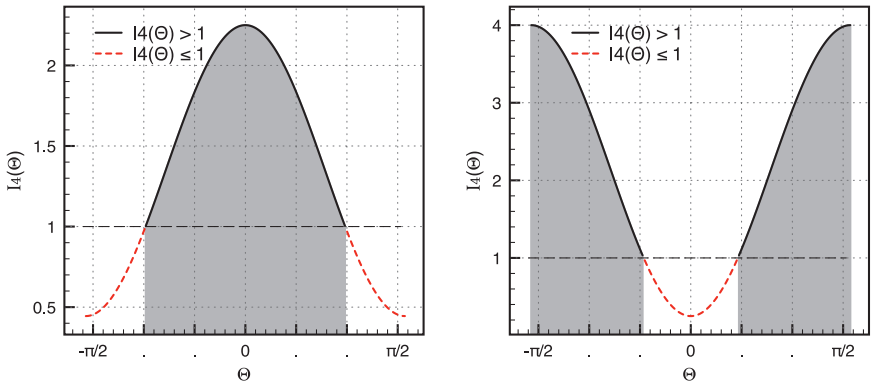

Fig. 11. Planar distributions, uniaxial loading. Plot of $I_4(\Theta)$, Eq. (44), the admissible ranges of Θ are denoted by the shadowed regions.

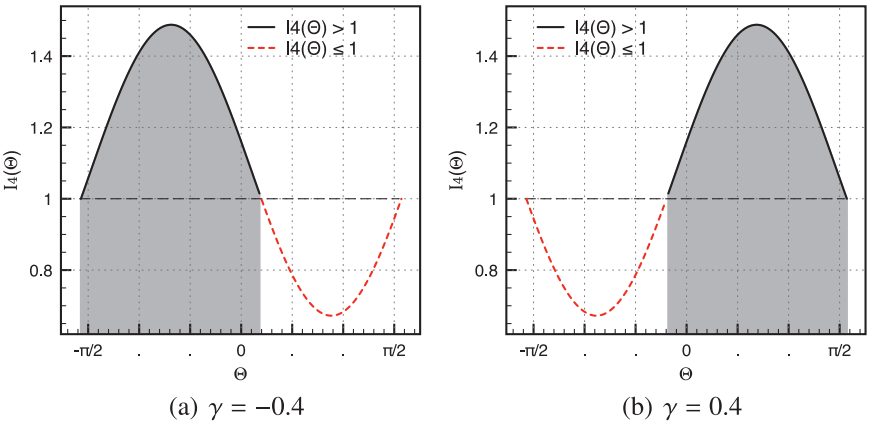

Fig. 12. Planar distributions, simple shear loading. Plot of $I_4(\Theta)$, Eq. (48), the admissible ranges of Θ are denoted by the shadowed regions.

For a given γ , the inversion of Eq. (48) can be done piecewise, obtaining the two contiguous functions:

$$\Theta_{1,2} = \frac{\gamma \pm \sqrt{\gamma^2 I_4 - (I_4 - 1)^2}}{I_4 - 1}. \tag{50}$$

Following the same analytical steps presented in the previous sections, we reach closed-form expressions for the PDF of I_4 and Ψ in the simple shear case as

$$\rho_{I_4}(I_4) = \frac{1}{N_{I_4}(\gamma, b)} \frac{\rho_\Theta(\theta)}{2\gamma(\cos^2\theta - \gamma \sin 2\theta)}, \tag{51}$$

where Θ is defined in Eq. (50), and

$$\rho_\Psi(\Psi) = \frac{1}{N_\Psi(\gamma, b)} \frac{\rho_{I_4}(I_4)}{k_1(I_4 - 1)\exp\left[k_2(I_4 - 1)^2\right]}\bigg|_{I_4 = I_4(\Psi)}, \tag{52}$$

where we assume $I_4 = I_4(\Psi)$ as in Eq. (31).

6. Numerical verification of the analytical results for uniaxial loading

In the previous sections, for selected loading cases of relevance in practical applications of transversely isotropic tissues, we derived the analytical expression of the PDF of the fourth pseudo-invariant and of the strain energy density. Moreover, using approximated forms of the strain energy density, we derived the analytical expression of the stress.

In this section, for the uniaxial loading case, we want to establish a quantitative comparison between the fourth pseudo-invariant, the strain energy density, and the stress components computed considering only the fibers in extension and the ones computed considering also the contribution of fibers in contraction. When possible and significant, in the calculations we alternate the use of the three PDFs, $\rho_\Theta(\theta)$, $\rho_{I_4}(I_4)$, $\rho_\Psi(\Psi)$, in the forms reported in Eqs. (23), (28), and (32), respectively. We observe that replacing the PDF in the definition of the fourth pseudo-invariant, strain energy density, and average stress, leads to the same results only when these quantities are computed over the support $\mathcal{D}_E$ including only the fibers in extension.

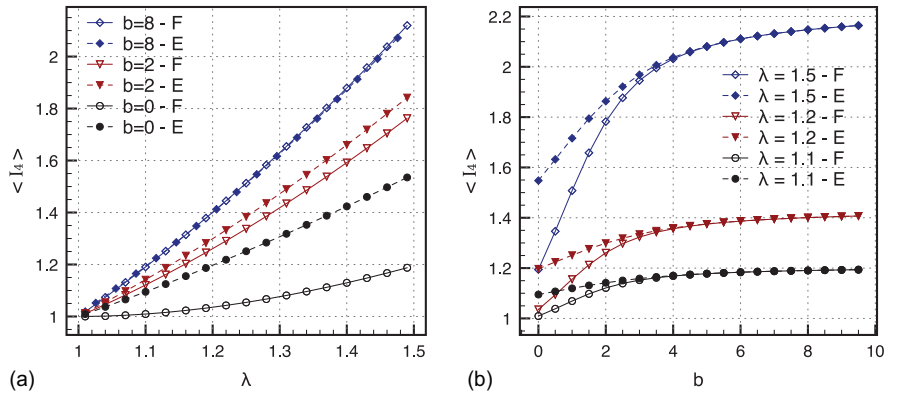

Fig. 13. Tridimensional distributions, uniaxial loading, numerical validation. Plots of the average $\langle I_4 \rangle$, computed over the full support $\mathcal{D}_F$ (F) and over the purely extended fiber support $\mathcal{D}_E$ (E). (a) $\langle I_4 \rangle$ versus stretch λ for fixed b. (b) $\langle I_4 \rangle$ versus $b = 0, 2, 3$ for fixed stretch $\lambda = 1.1, 1.2, 1.5$. The same curves are obtained using $\rho_\Theta(\theta)$ or $\rho_{I_4}(I_4)$. The full support underestimates the average value. The two integration schemes coincides for $b \gg 1$.

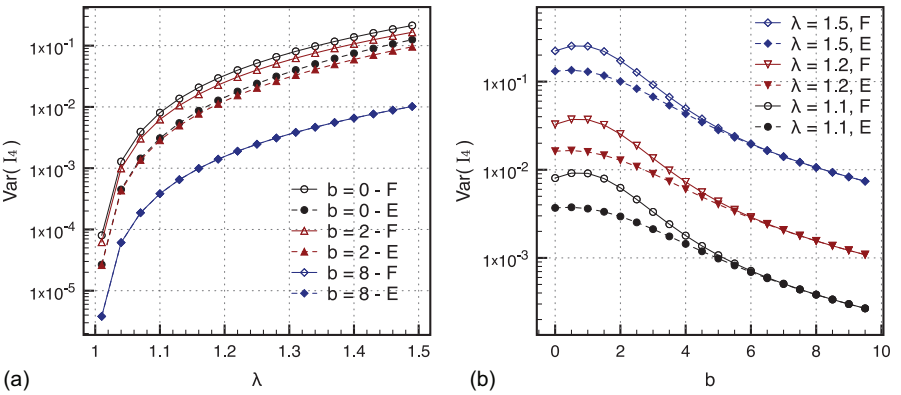

Fig. 14. Tridimensional distributions, uniaxial loading, numerical validation. Semi-log plots of the variance $\sigma^2_{I_4} = \mathrm{var}(I_4)$, computed over the full support $\mathcal{D}_F$ and over the purely extended fiber support $\mathcal{D}_E$. (a) $\sigma^2_{I_4}$ versus the stretch λ for fixed values of the concentration parameter $b = 0, 2, 8$. (b) $\sigma^2_{I_4}$ versus the concentration parameter b for fixed stretches $\lambda = 1.1, 1.2, 1.5$. The full support overestimates the variance value. The two integration schemes coincides for $b \gg 1$.

Fig. 13 illustrates the behavior of the average pseudo-invariant I^*_4, Eq. (17), computed using either $\rho_\Theta(\theta)$ or the PDF in Eq. (16). The plots show I^*_4 versus the stretch λ for fixed values of b, Fig. 13(a), and versus the concentration parameter b for fixed values of λ, Fig. 13(b). The curves are computed over the full support $\mathcal{D}_F$ (open symbols, F) and over the pure extension support $\mathcal{D}_E$ (full symbols, E). When the contracted fibers are excluded, I^*_4 assumes higher values; at high levels of alignment all curves superpose, since all fibers experience extension.

Fig. 14 shows the pseudo-invariant variance $\sigma^2_{I_4}$, see Eq. (18), computed over the full support $\mathcal{D}_F$ (open symbols, F) and over the pure extension support $\mathcal{D}_E$ (full symbols, E) using either $\rho_\Theta(\theta)$ or the PDF in Eq. (16). The semi-log variance $\sigma^2_{I_4}$ is plotted versus the stretch λ for fixed values of b, Fig. 14(a), and versus the concentration parameter b for fixed values of λ, Fig. 14(b). In all curves, $\sigma^2_{I_4}$ computed considering only the fibers in extension assumes smaller values. The maximum value for the variance is obtained for $b \simeq 1$; for high values of b all curves superpose and the restricted range becomes meaningless, all fibers being in extension.

Fig. 15 compares the average strain energy density $\langle \Psi \rangle$, computed over the full support, $\mathcal{D}_F$, and over the pure extension support, $\mathcal{D}_E$, using the PDF in Eq. (32). Starting from the Taylor expansion of Eq. (19), the energy associated to the direction Θ is approximated at two different levels: (i) us-ing the first order approximation, see Gasser et al., 2006; and (ii) using the second order approximation, see (Vasta et al., 2014). In the plots, the first and second approximation curves are labeled with G and V, respectively. Fig. 15(a–c) show the average strain energy density versus the stretch λ at fixed values of b, and Fig. 15(d–f) show the average strain energy density versus the concentration parameter b at fixed values of λ. The plots show that the second order approximation (solid line) is very accurate also in the case of dispersed fibers (Vasta et al., 2014), and that the integration over the full support leads to large errors in the case of very dispersed fibers (open symbols). Furthermore, the difference between the two approximations vanishes for high values of b, although the imposed stretch has a strong influence on the mechanical response. Interestingly, averaging over $\rho_\Psi(\Psi)$ automatically excludes the fibers in contraction.

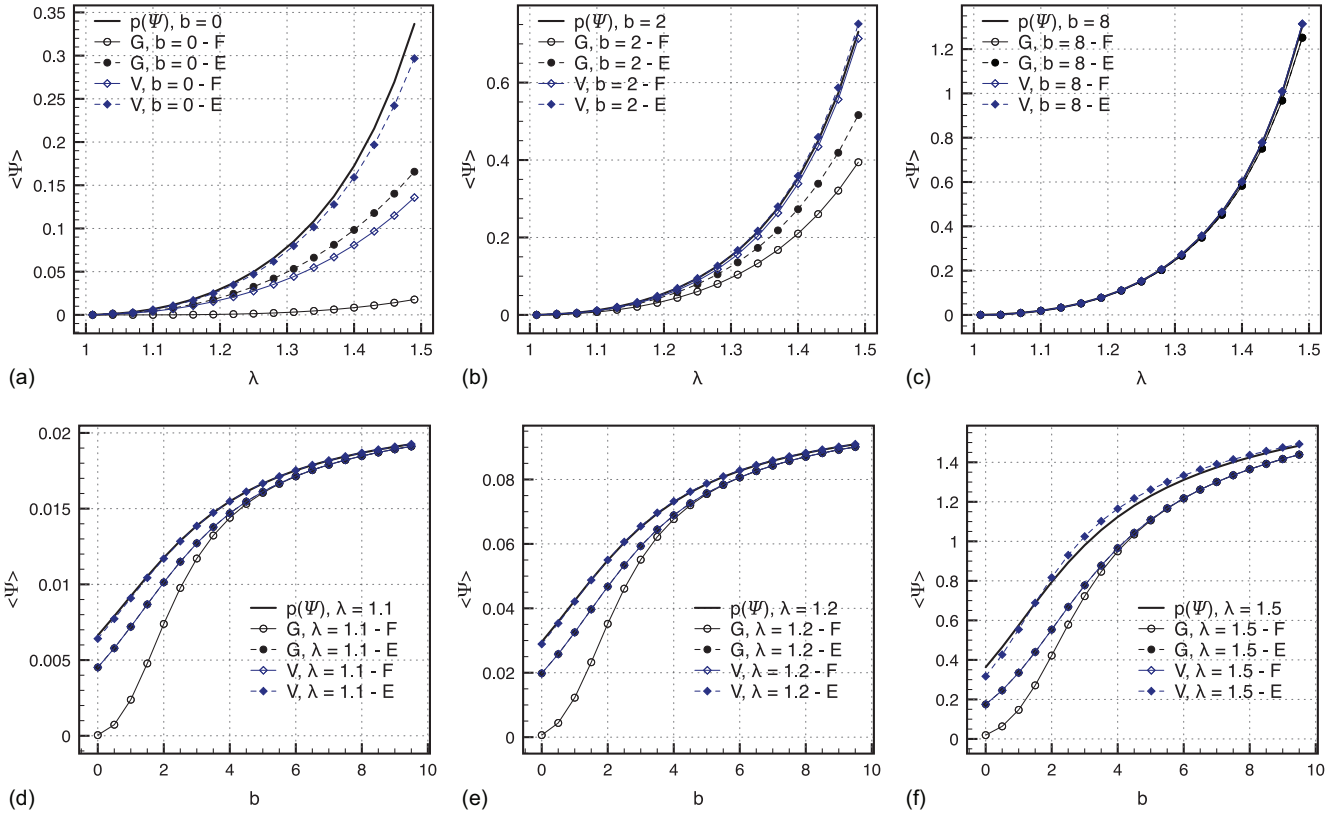

Fig. 15. Tridimensional distributions, uniaxial loading, numerical validation. Plots of the average $\langle\Psi\rangle$, computed over the full support $\mathcal{D}_F$ and over the purely extended fiber support $\mathcal{D}_E$ comparing the first (G) and second (V) order approaches. (a–c) $\langle\Psi\rangle$ versus the stretch λ for fixed values of the concentration parameter $b = 0, 2, 8$. (d–f) $\langle\Psi\rangle$ versus the concentration parameter b for fixed values of the stretch $\lambda = 1.1, 1.2, 1.5$. The full support underestimates the average value of the energy both in the first and second order approach. The second order approach better approximates the integral conducted directly with $\rho_\Psi(\Psi)$. The approximations coincides for $b \gg 1$.

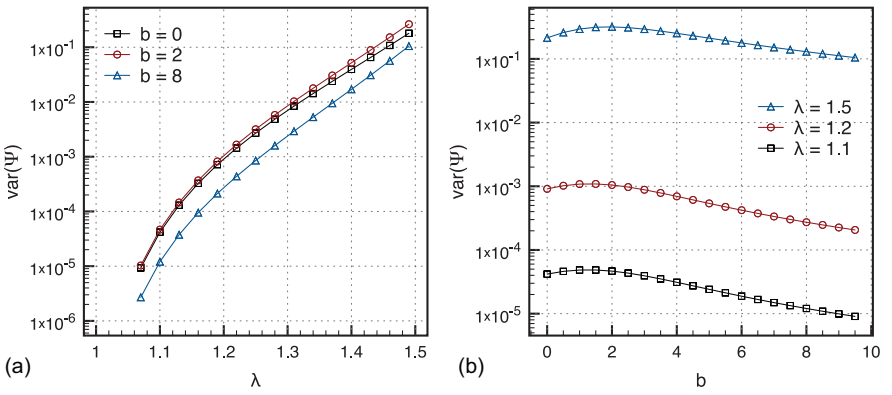

Fig. 16. Tridimensional distributions, uniaxial loading, numerical validation. Semi-log plots of the variance $\mathrm{var}(\Psi) = \langle \Psi - \Psi^* \rangle^2$ of the approximated strain energy density (a) versus stretch stretch λ for fixed values of the concentration parameter $b = 0, 2, 8$ and (b) versus b for fixed stretches $\lambda = 1.1, 1.2, 1.5$. Variance increases with stretch and shows a peak for $b \simeq 2$.

Fig. 16 visualizes the strain energy density variance $\sigma^2{}_\Psi$, Eq. (35), computed using the PDF in Eq. (32). The semi-log plots show σ^2_Ψ versus the stretch λ, Fig. 16(a), and versus the concentration parameter b, Fig. 16(b). For an assigned b, $\sigma^2{}_\Psi$ increases with increasing λ; as expected, the magnitude of the variance reduces with increasing b. The plot of σ^2_Ψ versus b for an assigned λ is characterized by a maximum at $b \simeq 2$ followed by a decreasing branch; the variance, though, is very sensitive to the magnitude of the stretch.

The plots in Fig. 17 show $\langle S_{33} \rangle$, the component in the load-ing direction of the average stress tensor, versus the stretch λ and the concentration parameter b, computed over the full, $\mathcal{D}_\mathrm{F}$, and the pure extension, $\mathcal{D}_\mathrm{E}$, supports. The stress is evaluated according to the definition in Eq. (22), using the first (G) and second (V) order approximations of the strain energy density. At low values of b the stress is very sensitive to the chosen model, and the second order approximation reproduces closely the exact average stress values. As expected, all the differences in the definition disappear at high values of b.

7. Discussion

The mechanical characterization of soft materials reinforced with distributed fibers cannot rely on deterministic approaches, which are often unsuitable and may lead to unrealistic predictions. Statistical approaches offer the correct tools to define the mechanical quantities necessary to obtain predictive and reliable models in numerical applications.

In this study, we consider distributions of fibers in tridimensional and planar settings, assuming radial symmetry about the main direction of the fiber orientation, typical of transversely isotropic materials. We restrict our attention to material models dependent only on the fourth pseudo-invariant I_4, a sort of microstructure-based measure of the local strain, corresponding to the square of the stretch in the direction of the fibers. Clearly, the complexity of fibrous materials may require the use of additional pseudo-invariants, such as I_5 or I_8 (Spencer, 1972), but in principle the present discussion can be extended to include additional strain measures, provided that the ensuing mathematical complexity can be worked through.

We begin from the hypothetically known and smooth PDF of the fiber orientation distribution, $\rho_\Theta(\theta)$, and, for loading conditions of particular interest for transversely isotropic materials, we derive analytically the expression of the PDF of the fourth pseudo-invariant, $\rho_{\mathrm{I}_4}(I_4)$, and of the strain energy density, $\rho_\Psi(\Psi)$. The PDFs are smooth functions, continuous and differentiable within the range of variability of the corresponding aleatoric variables, and characterized by a well defined support. Nevertheless, the fact that fibers fail to contribute to the material stiffness when in contraction imposes a restriction on the admissible values of the fourth pseudo-invariant, i.e., $\mathrm{I}_4 \geq 1$. This restriction affects the definition of the support of each PDF in a manner that depends unavoidably on the loading conditions.

Under *uniaxial loading*, the distinction between the full support and the support restricted to the fibers in pure extension leads to significant differences in the values of the κ and $\hat{\kappa}$ parameters that characterize first and second order approximations of the strain energy density. Both parameters are smaller if the pure extension range is considered, see Fig. 6. Strongly aligned fibers, i.e., high values of b, deliver smaller values of κ and $\hat{\kappa}$. The reduction of κ and $\hat{\kappa}$ signi-fies that the "active" portion of fibers contributing effectively to the mechanical response is less dispersed than the whole distribution of fibers. Another observation stems from the definition of stretch, a quantity that by definition is positive. Although all the contributions of the fiber bundles to I_4 are positive, in the case of full support the average operator in Eq. (5) is applied to a wider domain. In the wider domain fiber contributions assume values inferior to one, lowering the value of the average fourth pseudo-invariant, see Fig. 13. Likewise, also the component of the average stress in the direction of the loading assumes higher values in the case of restriction to the extended fibers.

Unfortunately, under general loading conditions it is not straightforward to obtain an analytical expression of the pure extension ranges, regardless to the fact that the mathematical basis for their definition is well understood (Holzapfel and Ogden, 2015). Pure extension ranges might be evaluated accurately through the analysis of the PDF of the strain energy density, $\rho_\Psi(\Psi)$, obviously only when the PDF is available in closed-form. In particular, $\rho_\Psi(\Psi)$ assumes a unique closed-form definition only for the pure extension ranges,

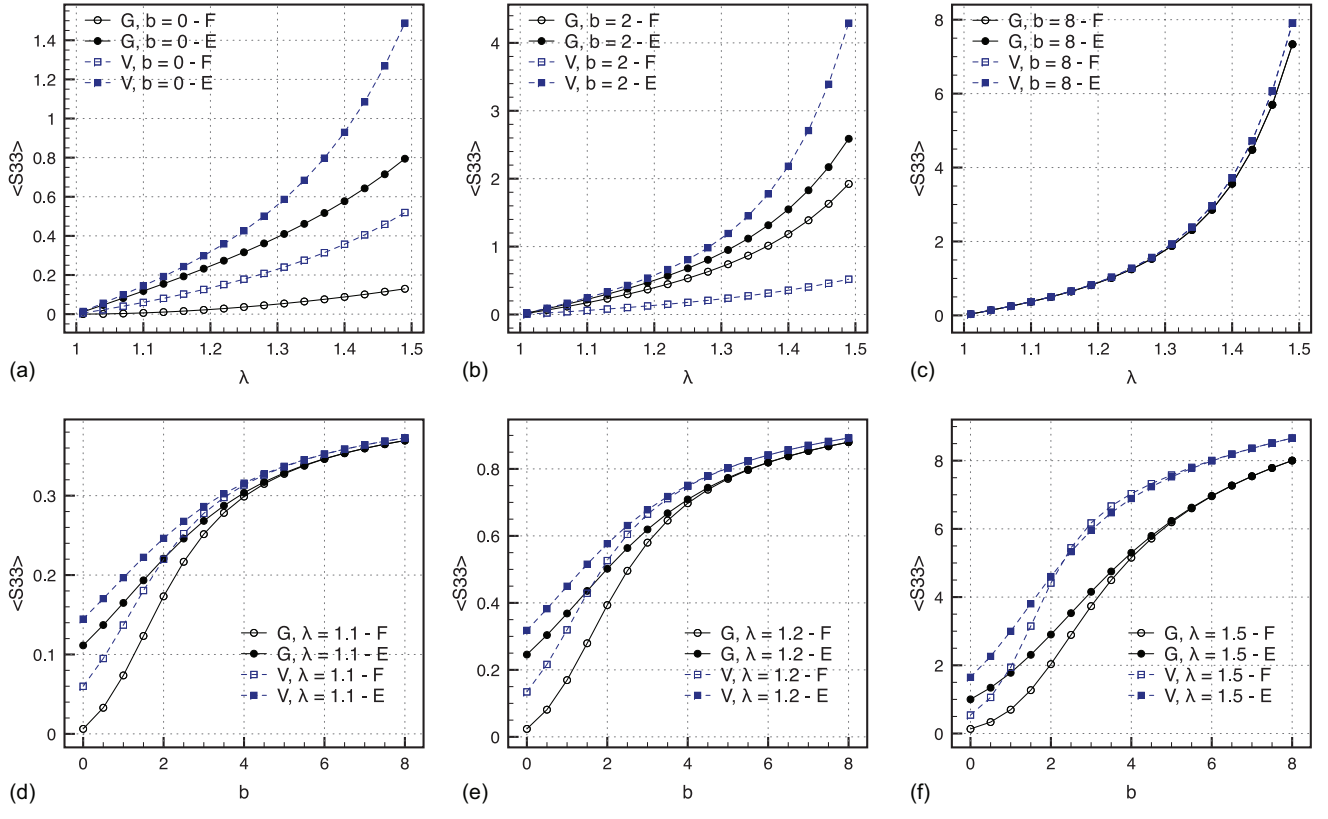

Fig. 17. Tridimensional distributions, uniaxial loading, numerical validation. Plots of the average $\langle S_{33}\rangle$, Eq. (22), computed on the full support $\mathcal{D}_F$ and on the extension support $\mathcal{D}_E$ comparing the first (G) and second (V) order approaches. (a–c) $\langle S^{33}\rangle$ versus stretch stretch λ for fixed $b = 0, 2, 8$. (d–f) $\langle S^{33}\rangle$ versus b for fixed stretch $\lambda = 1.1, 1.2, 1.5$. The average stress is underestimated by the full support. The two approaches coincides for $b \gg 1$.

i.e. $I_4 \geq 1$. The differences in κ, $\hat{\kappa}$, average energy, and average stress components vanish, in fact, if the pure extension ranges are considered. It is worth to note that in the definition of $\rho_\Psi(\Psi)$, Eq. (32), any functional form of $\rho_{I_4}(I_4)$ can be used. This possibility bestows the proposed formulation on a wide spectrum of material models.

Although the application of *general multiaxial loadings* for tridimensional distributions of fibers follows the same general transformation rule for random variables, this does not allow, in general, a handy derivation of analytical expressions of the PDFs. Neverthless, it is always possible visualize the dependence of I_4 on the Euler angles Θ and Φ by means of angle plane plots, see Fig. 5(b–f). The geometrical and topological complexity of the regions characterized by $I_4 \geq 1$ is a forerunner of the complexity of the analytical procedure to be carried out in order to obtain the desired PDFs. The PDF of the fourth pseudo-invariant is obtained in closed form for the general biaxial case, $\rho_{I_4}(I_4)$, Eq. (39). Due to the nonlinear interplay between the two principal stretches, the $\rho_{I_4}(I_4)$ possesses a non-monotonic behavior, see Fig. 9.

For planar distributions of the fibers, we obtained the closed-form of the PDFs for *uniaxial loading* which can be directly compared with the corresponding case for tridimensional fiber distribution. Differences between the two cases leap out from the comparison of Fig. 7(b) and Fig. 10(a). When the whole set of fibers lays on a plane, the contribution to a load on this plane is obviously more relevant, thus justifying the higher values reached by the PDFs.

8. Limitations and future perspectives

In this work, the generalized fourth invariant introduced in Holzapfel and Ogden (2015) has been derived analytically within a stochastic approach; a parametric study on the influence of the distribution parameter b and on the loading stretch λ has been carried out. There are some advantages in using an analytical formulation. For example, it is well known that the stability condition commonly used for generalized structure tensor models, i.e., $I^*_4 > 1$, can be satisfied also in the presence of a portion of compressed fibers. Nevertheless, for practical convenience in the absence of effective methods to exclude compressed fibers, this condition is used as a "switch" in well known commercial finite element software (Holzapfel and Ogden, 2015). The analytical definition of I_4 permits to define the ranges of the spatial angle Θ where the local condition $I_4 \geq 1$ is satisfied within the distribution, providing the correct definition of the PDFs of I_4 and Ψ. The closed-forms of $\rho_{I_4}(I_4)$ and $\rho_\Psi(\Psi)$ allow for the direct and correct evaluation of the requisite statistics (average and variance) of the fourth pseudo-invariant and of the strain energy density.

The approach discussed here has the following merits. (i) Enforcing the stability condition $I_4 \geq 1$ in terms of the PDF of the Euler angles requires complex curvilinear integrations (see Fig. 5). On the contrary, when the PDF of I_4 is available, the integration is straightforward just considering the support of $\rho_{I_4}(I_4)$ for $I_4 \geq 1$. This result has obvious important implications for the optimization of numerical schemes. (ii) The explicit derivation of the PDF of I_4, $\rho_{I_4}(I_4)$, requires in general a piece-wise inversion procedure. Although inversion could introduce analytic difficulties, the explicit knowledge of the PDF permits to obtain its statistics up to any order, thus delivering a wider information than the average. The availability of higher order statistics opens the possibility to further ex-tensions and applications to methods based on the use of generalized high-order structure tensors. As remark-able example, an interesting avenue has been recently addressed in Cortes and Elliot (2014), where I_4's central statistics of any order have been used. (iii) The additional possibility to obtain the PDF of the energy, and eventually the energy statistics, opens new and interesting perspectives for novel generalized formulations.

The exact quantification of the distribution parameters is instrumental for the statistical characterization of fiber reinforced material models and for the reliability of computational methods based on those models. As already mentioned, given their particular microstructure and individual variability, biomaterials and biotissues do require a statistic approach.

A possible extension of this study is the characteriza-tion of the PDF for multi-axial loadings, that cannot be de-rived in a handy analytical form, by means of advanced *ad hoc* computational tools, e.g., Monte Carlo simulations. An-other point that would merit some further investigation is the achievement of a closed-form of the stress tensor. Its analytical derivation involve complex integral derivatives with a variable integration domain, thus requiring with additional terms due to Leibniz integral rule, see e.g. (Vasta et al., 2014). Finally, a valuable aspect of this study is that the discussed approach can be directly generalized to any experimental-based statistical distribution of fiber-reinforced materials. In particular, multi-modal distributions, already identified in numerous biological tissues, appear as optimal candidates.

Competing interests

We have no competing interests.

Funding

The authors acknowledge the Gruppo Nazionale per la Fisica Matematica (GNFM), INdAM, for partial supporting this work under the Young Researcher Grant 2014.

Appendix A. Fourth order tensor $\mathbb{H}$

The fourth order structure tensor $\mathbb{H}$ is defined as (Pandolfi and Vasta, 2012):

$$\mathbb{H} = \langle \mathbf{A} \otimes \mathbf{A} \rangle,$$

with non zero coefficients:

$$\begin{aligned} H_{1111} = H_{2222} &= 3\hat{\kappa}, \\ H_{3333} &= 1 - 4\kappa + 8\hat{\kappa}, \\ H_{1122} = H_{2211} = H_{1212} = H_{2121} = H_{1221} = H_{2112} &= \hat{\kappa}, \\ H_{2233} = H_{3322} = H_{2323} = H_{3232} = H_{2332} = H_{3223} &= \kappa - 4\hat{\kappa}, \\ H_{3311} = H_{1133} = H_{3131} = H_{1313} = H_{3113} = H_{1331} &= \kappa - 4\hat{\kappa}. \end{aligned}$$

Functions f, g in Eq. (22), with $\Psi^* = \Psi(I^*_4)$, are defined as

$$f(I^*_4, \sigma^2_{I_4}) = \Psi^* \sum_j^{0..3} a_j I^{*j}_4 \quad g(I^*_4, \sigma^2_{I_4}) = \Psi^* \sum_j^{0..2} b_j I^{*i}_4.$$

The non zero coefficients of the second order stress tensor **S** are (see Vasta et al., 2014):

$$a_0 = -4k_2 - 8\sigma_{I_4}^2 2k_2^3 - 12\sigma_{I_4}^2 2k_2^2\,, \qquad b_0 = 4k_2 + 8k_2^2\,,$$
$$a_1 = 24\sigma_{I_4}^2 2k_2^3 + 12\sigma_{I_4}^2 2k_2^2 - 8k_2^2\,, \qquad b_1 = -16k_2^2,$$
$$a_2 = 16k_2^2 - 24\sigma_{I_4}^2 2k_2^3\,, \qquad b_2 = 8k_2^2,$$
$$a_3 = 8\sigma_{I_4}^2 2k_2^3 - 8k_2^2.$$

References

Alastrué, V., Rodríguez, J.F., Calvo, B., Doblaré, M., 2007. Structural damage models for fibrous biological soft tissues. Int. J. Solids Struct. 44, 5894–5911.

Arruda, E.M., Boyce, M.C., 1993. A three-dimensional constitutive model for the large stretch behavior of rubber elastic materials. J. Mech. Phys. Solids 41, 389–412.

Casella, G., Berger, R., 2008. Statistical Inference. Brooks/Cole.

Cortes, D.H., Elliot, D.M., 2014. Accurate prediction of stress in fibers with distributed orientations using generalized high-order structure tensors. Mech. Mater. 75, 73–83.

Driessen, N.J., V., B.C., Baaijens, F.P., 2005. A structural constitutive model for collagenous cardiovascular tissues incorporating the angular fiber distribution. J. Biomech. Eng. 127, 494–503.

Federico, S., Gasser, T.C., 2010. Nonlinear elasticity of biological tissues with statistical fibre orientation. J. R. Soc. Interface 7, 955–966.

Ferrara, A., Pandolfi, A., 2008. Numerical modeling of fracture in human arteries. Comput. Methods Biomech. Biomed. Eng. 11, 553–567.

Fisher, N., Lewis, T., Embleton, B., 1987. Statistical Analysis of Spherical Data. Cambridge University Press, Cambridge.

Gasser, T.C., Ogden, R.W., Holzapfel, G.A., 2006. Hyperelastic modeling of arterial layers with distributed collagen fibre orientations. J. R. Soc. Interface 3, 15–35.

Gizzi, A., Vasta, M., Pandolfi, A., 2014. Modeling collagen recruitment in hyperelastic bio-material models with statistical distribution of the fiber orientation. Int. J. Eng. Sci. 78, 48–60.

Holzapfel, G.A., Gasser, T.C., Ogden, R.W., 2000. A new constitutive framework for arterial wall mechanics and a comparative study of material models. J. Elast. 61, 1–48.

Holzapfel, G.A., Ogden, R.W., 2015. On the tension-compression switch in soft fibrous solids. Eur. J. Mech. Solids 49, 561–569.

Horgan, C.O., Saccomandi, G., 2003. A description of arterial wall mechanics using limiting chain extensibility constitutive models. Biomech. Model. Mechanobiol. 1, 251–266.

Lanir, Y., 1983. Constitutive equations for fibrous connective tissues. J. Biomech. 16, 1–12.

Li, D., Robertson, A.M., 2009. A structural multi-mechanism constitutive equation for cerebral arterial tissue. Int. J. Solids Struct. 46, 2920–2928.

Mardia, K.V., Jupp, P.E., 2000. Directional Statistics. John Wiley & Sons Ltd, Chichester.

Ni Annaidh, A., Bruyere, K., Destrade, M., Gilchrist, M.D., Maurini, C., Ottenio, M., Saccomandi, G., 2012. Automated estimation of collagen fibre dispersion in the dermis and its contribution to the anisotropic behaviour of skin. Ann. Biomed. Eng. 40, 1666–1678.

Pandolfi, A., Vasta, M., 2012. Fiber distributed hyperelastic modeling of biological tissues. Mech. Mater. 44, 151–162.

Rodríquez, J.F., Cacho, F., Bea, J.A., Doblaré, M., 2006. A stochastic-structurally based three dimensional finite-strain damage model for fibrous soft tis-sue. J. Mech. Phys. Solids 44, 864–886.

Sacks, M.S., 2003. Incorporation of experimentally-derived fiber orientation into a structural constitutive model for planar collagenous tissues. J. Biomech. Eng. - Trans. ASME 125, 280–287.

Sánchez, P., Moutsouris, K., Pandolfi, A., 2014. Biomechanical and optical behavior of human corneas before and after photorefractive keratectomy. J. Cataract Refract. Surg. 40, 905–917.

Spencer, A.J.M., 1972. Deformations of Fibre Reinforced Materials. Oxford Science Research Papers, Oxford.

Tsamis, A., Krawiec, J.T., Vorp, D.A., 2013. Elastin and collagen fibre microstructure of the human aorta in ageing and disease: a review. J. R. Soc. Interface 10, 20121004.

Vasta, M., Gizzi, A., Pandolfi, A., 2014. On three- and two-dimensional fiber distributed models of biological tissues. Probab. Eng. Mech. 37, 170–179.

Wang, Y., Son, S., Swartz, S.M., Goulbourne, N.C., 2012. A mixed von-mises distribution for modeling biological tissues with two distributed fiber properties. Int. J. Solids Struct. 49, 2914–2923.

Zulliger, M.A., Rachev, A., Stergiopulos, N., 2004. A constitutive formulation of arterial mechanics including vascular smooth muscle tone. Am. J. Physiol. Heart Circ. Physiol. 287, H1335–H1343.